Available online at www.sciencedirect.com
ScienceDirect
Cement and Concrete Research 38 (2008) 226–246
Cement and Concrete Research

Durability of concrete — Degradation phenomena involving detrimental chemical reactions

Fredrik P. Glasser [a], Jacques Marchand [a,b,*], Eric Samson [c]

[a] Department of Chemistry, University of Aberdeen, UK
[b] CRIB-Department of Civil Engineering, Laval University, Canada
[c] SIMCO Technologies, Canada

Received 28 August 2007; accepted 10 September 2007

Abstract

While interacting with its service environment, concrete often undergoes significant alterations that often have significant adverse consequences on its engineering properties. As a result, the durability of hydrated cement systems and their constituent phases has received significant attention from scientists and engineers. Cement paste deterioration by detrimental chemical reactions is discussed. First, the mechanisms that govern the transport of ions, moisture and gas are described. Then, different chemical degradation phenomena are reviewed. Microstructural alterations resulting from exposure to chlorides and carbon dioxide are discussed. Sulfate attack from external sources is described including processes resulting in the formation of ettringite and thaumasite. The mineralogy of Portland cement is sensitive to temperature and thermal cycling, particularly during the early hydration period.

Keywords: Durability

1. Introduction

The good durability of Portland cement compositions in normal service environments has long been recognized. However, cements and concretes made with cement binders can be attacked and, as a result, exhibit a reduced service life. Most of the adverse conditions are recognized from experience and have been the subject of numerous examinations of field concretes as well as laboratory studies. Not surprisingly, research and testing have focused on the areas of underperformance.

The concept of a "service life" is not new. The ancient world used stone, brick, tile and, from Roman times onwards, concrete, because of their permanence. Today, cement and Portland cement concrete are widely used and comprise the world's major structural material.

Although modern cements are much improved in properties, the high and rising cost of construction and the economic cost and disruption associated with replacement and renewal, especially of major infrastructure facilities, placed new pressures on ensuring durable construction. Again, these pressures are not new but have intensified particularly in view of the relatively high carbon penalty associated with cement production and use.

The perceived problems arising from limited performance have long been the subject of investigation. Most of this has been empirical in nature although often employing sophisticated statistical controls. We have also seen the rise of modeling, as a way of predicting durability and compressing the time factor without distortion of the underlying mechanisms.

Thus the art and science of durability are in a state of great activity with the development of a variety of approaches. This is healthy. But we have so much of significance to report that this review can only capture selected aspects of current research.

2. Transport mechanisms

2.1. Ionic transport

The development of ionic transport models has initially been motivated by concerns over the premature degradation of concrete structures exposed to chloride-laden environments. Early models

* Corresponding author. CRIB-Department of Civil Engineering, Laval University, Canada.
E-mail address: Jacques.Marchand@gci.ulaval.ca (J. Marchand).

0008-8846/$ - see front matter © 2007 Published by Elsevier Ltd.
doi:10.1016/j.cemconres.2007.09.015

were typically limited to simplified equations describing the diffusion of a single ion (e.g. chloride) in saturated concrete. These simple models were gradually improved to account for the complexity of ionic transport in unsaturated systems. Multi-ionic models that consider not only diffusion but other transport mechanisms, such as water movement under the effect of humidity gradients, were proposed and tested.

The description of transport phenomena is usually performed by writing the mass conservation equations at the pore level. The equations are then averaged over a Representative Elementary Volume (REV) of the material. By solving the averaged mass transport equations, one can therefore perform simulations at the scale of the concrete element.

At the pore scale, it is typically assumed that ions can be transported by a combination of two phenomena: an electrochemical potential gradient and the advection caused by a flow of the aqueous solution [1,2]:

$$\mathbf{j}_i = \underbrace{-\frac{D_i^o}{RT} c_i \mathrm{grad}(\mu_i)}_{\text{electrochemical}} + \underbrace{c_i \mathbf{v}}_{\text{advection}} \tag{1}$$

where c_i is the concentration of ionic species i, D_i^o is the diffusion coefficient in free water, μ_i is the electrochemical potential, R is the ideal gas constant, T is the temperature and $\mathbf{v}$ is the velocity of the liquid phase.

The electrochemical potential μ_i is defined as:

$$\mu_i = \mu_i^o + RT\ \ln(\gamma_i c_i) + z_i F \psi \tag{2}$$

where μ_i^o is a reference level, γ_i is the chemical activity coefficient, z_i is the valence number of the ionic species and ψ is the electrochemical potential. Substituting Eq. (1) in (2) yields [3]:

$$\mathbf{j}_i = -D_i^o \mathrm{grad}(c_i) - \frac{D_i^o z_i F}{RT} c_i \mathrm{grad}(\psi) - D_i^o c_i \mathrm{grad}(\ln\gamma_i) - \frac{D_i^o c_i \mathrm{grad}(\ln\gamma_i)}{T} \mathrm{grad}(T) + c_i \mathbf{v} \tag{3}$$

Each term on the right-hand side of Eq. (3) corresponds to a different mechanism. The first term, often called the diffusion term or Fick's law, describes the movement of ionic species under the effect of a concentration gradient.

The second term involving the electrochemical potential is responsible for maintaining the pore solution electroneutrality by slightly altering the velocity of individual species. The electrochemical potential thus couples each individual flux equation [4].

The chemical activity term is essentially a correction to the flux when the ionic strength of the pore solution is high. The chemical activity term in Eqs. (2) and (3) can be estimated using an equation that relates the chemical activity coefficient γ_i to the concentrations in solution. Classical electrochemical models like the Debye–Hückel or extended Debye–Hückel relationships are valid for weak electrolytes for which the ionic strength is on the order of 100 mmol/L, while the Davies correction can be used to describe the behavior of more concentrated solutions, i.e. with ionic strengths up to 300 mmol/L [5]. Pore solutions extracted from hydrated cement systems are more in the 300 mmol/L [6] to 900 mmol/L range [7]. Pitzer's model was used by Reardon [8] to model the paste/solution chemical equilibrium. Samson & al. proposed a modification to Davies' model [9] that allows calculating the chemical activity coefficients for 1 mol/L ionic strength solutions:

$$\ln\gamma_i = \frac{-Az_i^2\sqrt{I}}{1 + a_i B\sqrt{I}} + \frac{\left(0.2 - 4.17\times10^{-5} I\right) A z_i^2 I}{\sqrt{1000}} \tag{4}$$

where A and B are temperature dependent parameters and a_i is an ion-dependent parameter. Li and Page [10] proposed another type of relationship to evaluate the mean natural logarithm activity coefficient:

$$\frac{1}{N}\sum_{i=1}^{N} \ln\ \gamma_i = \alpha\left(\frac{2}{3}\sqrt{\frac{I}{I_{cr}}} - 1\right) I \tag{5}$$

where I_{cr} is called the critical ionic strength. For $I > I_{cr}$, the mean natural logarithm activity coefficient increases with the ionic strength of the solution, whereas it decreases for $I < I_{cr}$. The value of the parameter α depends on the I/I_{cr} ratio.

The next term in Eq. (3), which involves temperature, is called the Soret effect. It describes the influence of a temperature gradient on the ionic flux.

The constitutive Eq. (3) can be simplified in some specific cases. For instance, for isothermal cases, the term associated with the temperature gradient can be neglected.

To get the complete transport equation, the constitutive Eq. (3) is substituted in the mass conservation relationship [11]:

$$\frac{\partial c_i}{\partial t} + \mathrm{div}(j_i) + r_i = 0 \tag{6}$$

where r_i is the reaction rate term accounting for complexation in the solution. The complexation reactions are taking place solely within the aqueous phase. The formation of $CaOH^+$ is an example of complexation reaction: $Ca^{2+} + OH^- \rightleftarrows CaOH^+$. At the pore scale, the other types of chemical reactions, i.e. dissolution/precipitation and surface adsorption, could be modeled by exchange terms at the aqueous/solid interface.

Combining Eqs. (3) and (6) gives the complete ionic transport equation in the aqueous phase at the pore scale:

$$\frac{\partial c_i}{\partial t} - \mathrm{div}\left(D_i^o \mathrm{grad}(c_i) + \frac{D_i^o z_i F}{RT} c_i \mathrm{grad}(\psi) + D_i^o c_i \mathrm{grad}(\ln\ \gamma_i) + \frac{D_o^i c_i \mathrm{grad}(\ln\ \gamma_i)}{T} \mathrm{grad}(T) - c_i v\right) + r_i = 0 \tag{7}$$

However, modeling transport of ions at the pore scale is currently an impossible task. One would have to know the exact geometry of the entire porous network. Furthermore, the computational resources required to conduct these calculations are currently unavailable. To circumvent this difficulty, pore scale equations need to be averaged over the scale of the material. This can be achieved using a mathematical procedure called homogenization. The general application of the method can be found in references [11,12]. The technique was specifically applied to cement-based materials in reference

[13]. It should be noted that Johannesson [14] developed an ionic transport model on the basis of the mixture theory and obtained similar results. In the homogenization (or averaging) technique, equations are integrated over the Representative Elementary Volume (REV) to lead to the equations at the scale of the material. The averaged form of Eq. (7) is [3]:

$$\frac{\partial\left(\theta_s C_i^s\right)}{\partial t}+\frac{\partial(wC_i)}{\partial t}-\operatorname{div}\left(D_i w\operatorname{grad}(C_i)+\frac{D_i z_i F}{RT}wC_i\operatorname{grad}(\Psi)+D_i wC_i\operatorname{grad}(\ln\gamma_i)+\frac{D_i C_i\operatorname{grad}(\ln\gamma_i)}{T}w\operatorname{grad}(T)-C_i\mathbf{V}\right)+wR_i=0 \tag{8}$$

where the uppercase parameters represent the average of the corresponding quantities in Eq. (7). The averaging process introduces the volumetric water content w in the mass transport equation. Also, a term involving the solid phase fraction θ_s and the content of the ionic species i bound to the solid matrix, C_i^s is now part of the relationship. This term is often used to model chemical reactions between the pore solution and the hydrated cement paste. More details on the subject will be given in the following sections. On the contrary, the term R_i dedicated to homogeneous chemical reactions is always neglected.[1]

The parameter D_i in Eq. (8) is the diffusion coefficient at the macroscopic level. It can be related to D_i^o by the expression:

$$D_i=\tau D_i^o \tag{9}$$

where τ is the tortuosity of the aqueous phase, a purely geometrical factor accounting for the complexity of the porous network. Many authors have relied on this definition [3,11,16]. Other authors [17,18] elected to work instead with the following definition:

$$D_i=\frac{D_i^o}{\tau} \tag{10}$$

Several factors can affect the diffusion coefficient such as the degree of saturation of the material, the ambient temperature, and any modification to the pore structure of the material (either induced by continuing hydration or chemical reactions). As proposed by Saetta et al. [19], the different factors can be expressed as separate functions such as:

$$D_i=\tau D_i^o\times S(w)\times G(T)\times H(t)\times M(\phi) \tag{11}$$

The function $S(w)$ models the effect of the degree of saturation on the diffusion process. Few models have been developed specifically for cement-based materials. Samson and Marchand [3] used a relationship derived by Quirk and Millington for transport in groundwater:

$$S(w)=\frac{w^{7/3}}{\phi_o^{7/3}} \tag{12}$$

[1] The situation is different in groundwater transport, where the homogeneous reactions are an important part of the pollutant movement process (see for instance Ref. [15]).

where ϕ_o is the initial porosity of the material. In the approach developed by Saetta et al. [19], the function S is based on the relative humidity inside the material:

$$S(h)=\left(1+\frac{(1-h)^4}{(1-h_c)^4}\right)^{-1} \tag{13}$$

where h_c is the critical humidity threshold at which the diffusion coefficient loses half its value.

The effect of temperature has traditionally been considered using an exponential relationship that features the activation energy [19]:

$$G(T)=\exp\left[\frac{U}{R}\left(\frac{1}{T_o}-\frac{1}{T}\right)\right] \tag{14}$$

where U is the activation energy of the diffusion process and T_o is a reference temperature, usually around 25 °C. More recently, Samson et al. [3] derived an expression that was found to properly describe the effect of temperature on the transport of ions in different materials:

$$G(T)=e^{0.028(T-T^o)} \tag{15}$$

Similarly, different relationships have been developed to model the effect of hydration on diffusion. Some are listed here:

$$H(t)=\begin{cases}a+(1-a)\left(\dfrac{t^{ref}}{t}\right)^{1/2} & [19]\\ \left(\dfrac{t^{ref}}{t}\right)^{m} & [20]\\ \dfrac{a}{1+(a-1)e^{-\alpha\left(t-t^{ref}\right)}} & [3]\end{cases} \tag{16}$$

All these relationships have their maximum value early in the life of the material and decrease as the hydration process proceed. In most cases, t^{ref} is taken as 28 days. The relationships presented in references [3,19] converge to a as $t\to\infty$, whereas the one in reference [20] always decreases with time. The influence of continuous hydration on the transport properties of concrete can be particularly significant for mixtures prepared with supplementary cementing materials such as fly ash and granulated blast-furnace slag.

As previously mentioned, chemical reactions can locally modify the pore structure of concrete and its transport properties. For instance, the formation of new phases can lead to a reduction of the material's porosity and contribute to reduce its transport properties. Likewise, the dissolution of existing phases can open the pore space and increase the diffusion coefficient. A modified version of the Kozeny–Karman relationship is often used in groundwater transport to calculate the correction factor $M(\phi)$ that accounts for the effect of chemical alteration on the diffusion mechanism:

$$M(\phi)=\left(\frac{\phi}{\phi_o}\right)^3\left(\frac{1-\phi_o}{1-\phi}\right)^2 \tag{17}$$

Relationships specifically devoted to cement-based materials have not been a major research topic. The following relationship was proposed recently [21]:

$$M(\phi) = \left(\frac{e^{4.3\phi/V_p}}{e^{4.3\phi_o/V_p}}\right) \tag{18}$$

where V_o is the paste volume of the material.

In order to solve the general ionic transport Eq. (8), other relationships are needed to evaluate the temperature, water content and electrochemical potential fields. These points are described in the following sections.

2.1.1. Moisture transport

Two main approaches have been used to model moisture movement in hydrated cement systems. The first one is based on a thorough description of all the phases involved in the process: liquid (aqueous solution), water vapor and dry air. Multiple mass conservation equations are involved to obtain the description of the global moisture fields. The second approach can be derived from the first one under simplifying assumptions. It usually leads to a single equation (called the Richards' equation), which allows the water content field to be evaluated. Both approaches are reviewed in the following paragraphs.

Mainguy et al. [22] relied on the multiphase approach to describe moisture movement under isothermal conditions. The mass balance equations for the three phases [liquid water (l), dry air (a) and water vapor (v)] that can be present in partially saturated concrete are given as:

$$\frac{\partial}{\partial t}(\phi\rho_l S_l) = -\mathrm{div}(\phi S_l \rho_l v_l) - \mu_{l\to v} \quad \text{(liquid)} \tag{19}$$

$$\frac{\partial}{\partial t}(\phi\rho_v(1-S_l)) = -\mathrm{div}(\phi(1-S_l)\rho_v v_v) + \mu_{l\to v} \quad \text{(water vapor)} \tag{20}$$

$$\frac{\partial}{\partial t}(\phi\rho_a(1-S_l)) = -\mathrm{div}(\phi(1-S_l)\rho_a v_a) \quad \text{(dry air)} \tag{21}$$

where ϕ is the porosity, ρ_i is the density of phase i, S_l is the liquid water saturation, v_i is the velocity of constituent i, and $\mu_{l\to v}$ is the rate of liquid water vaporization. The liquid phase velocity is given by the Darcy state law:

$$\phi v_i = -\frac{K}{\eta_i} k_{ri}(S_l)\mathrm{grad}(p_i) \tag{22}$$

where K is the intrinsic permeability of the porous material, η_i is the dynamic viscosity of phase i, $k_{ri}(S_l)$ is the relative permeability and p_i is the pressure. The dry air and vapor phases state laws are given by Fick's relationship, expressed as:

$$\phi_g \rho_j v_j = \phi_g \rho_j v_g - \rho_j \frac{D}{C_j} f(S_l,\phi)\mathrm{grad}\left(C_j\right) \tag{23}$$

where v_g is the gas molar-averaged velocity satisfying Darcy's law, D is the diffusion coefficient of water vapor or dry air in wet air, f is the resistance factor accounting for both the tortuosity effect and the reduction space offered to the diffusion of gaseous constituents, and C_j is the ratio p_j/p_g with $j=a$ or v [23]. A similar model was developed by Selih [24]. The model developed by Mainguy et al. [22], has been found to properly reproduce isothermal drying test results. However, this approach is marginally useful in durability analyses, mainly because of the rather large number of parameters that need to be determined.

The simplified approach is often selected to describe the variation in water content within cement-based materials. One of the main differences between two approaches is the assumption that gas pressure is uniform over the material and is equal to atmospheric pressure. Under this hypothesis, it has been shown [13,25] that the water content can be evaluated on the basis of Richards' equation:

$$\frac{\partial w}{\partial t} - \mathrm{div}(D_w \mathrm{grad}(w)) = 0 \tag{24}$$

where w is the volumetric water content and D_w is the nonlinear water diffusivity parameter. Using this approach, the velocity of the fluid phase appearing in Eq. (8) is given by:

$$V = -D_w \mathrm{grad}(w) \tag{25}$$

It is commonly accepted that D_w follows an exponential relationship [26]: $D_w = A\ \exp(B \times w)$, where B is positive. Instead of using water content as state variable, other authors have elected to model the relative humidity field h, under the assumption that the driving force can be expressed as: $V = -D_h \mathrm{grad}(h)$. In that case, Eq. (24) can be written as [27,28]:

$$\frac{\partial w}{\partial h}\frac{\partial h}{\partial t} - \mathrm{div}(D_h \mathrm{grad}(h)) = 0 \tag{26}$$

Again, the moisture diffusivity parameter is a nonlinear function that can be expressed as [28]:

$$D_h = \alpha + \beta\left(1 - 2^{-10\gamma(h-1)}\right) \tag{27}$$

where α, β and γ are parameters that need to be determined experimentally.

2.1.2. Electrochemical potential

Many ionic transport models neglect the electrochemical potential and the electrical coupling between ions. This is the case in groundwater modeling, where the ionic concentration levels are typically relatively low, at least compared to the pore solution of hydrated cement systems. Until recently, this was accepted as applicable to ionic diffusion in concrete. However, some recent models are now considering coupling effects, assuming that the high concentration levels in the pores may cause strong concentration gradients, in which case the electrochemical potential term in the mass conservation equation is no longer negligible. Some of these models will be reviewed when specific degradation mechanisms are addressed.

Two different approaches have been used to solve the electrochemical potential issue. The first one relies on the null current density hypothesis $\sum_i z_i j_i = 0$ to eliminate the electrochemical potential from the transport equation. This approach

was taken by Truc et al. [29] and Masi et al. [30]. The electrochemical potential can also be taken into account with the use of Poisson's equation that directly relates the potential to the concentration in solution. It is given here in its averaged form [13]:

$$\mathrm{div}(w\tau \mathrm{grad}(\Psi)) + w\frac{F}{\varepsilon}\left(\sum_{i=1}^{N} z_i C_i\right) = 0 \quad (28)$$

where ε is the permittivity of the solution (usually assumed to be the same as water) and N is the total number of ionic species in aqueous phase. The coupling of Poisson's equation with the ionic transport relationship was used in references [3,14] to model ionic transport.

2.1.3. Temperature field modeling

Different modeling approaches have been proposed to predict temperature distribution in porous materials. The most comprehensive consists of resolving the energy balance equation for each phase in the porous medium. This approach was used by Schrefler [31] to model the temperature and humidity fields in concrete structures exposed to fire. The relationships are coupled through balance equations at the interfaces between each phase. However, these terms prove difficult to evaluate and are often neglected.

For most long-term durability analyses, the energy conservation equation can be simplified to the well-known heat conduction relationship:

$$\rho C_p \frac{\partial T}{\partial t} - \mathrm{div}(k\mathrm{grad}T) = 0 \quad (29)$$

where ρ is the density of the material, C_p is the heat capacity, and k is the thermal conductivity. As emphasized in Ref. [3], this relationship assumes that the heat of hydration effect are negligible after a few days, heat flow through convection caused by the fluid and gas movement in the material is negligible, and the heat capacity and conductivity parameter can be expressed as an average value of all the individual contribution of the various phases that compose the material. Eq. (28) has been used by a few authors [19,32] to evaluate the temperature field in concrete structures.

3. Chloride ingress and corrosion

As mentioned previously in the introduction, the ingress of chloride and its role in corrosion initiation is what prompted the development of the first models dedicated to long-term durability analyses of concrete structures. The following sections summarize the different mechanisms involved during chloride ingress and the modeling approaches described in the literature.

3.1. Chloride interaction with hydrated cement systems

It is generally accepted that the penetration of chloride in cement-based materials does not readily lead to the formation of detrimental solid phases that may cause expansion and cracking. On the contrary, the interaction between chloride in solution and the paste, because it binds penetrating ions, is often considered to have a beneficial influence on the durability of reinforced concrete since it slows the rate of ingress toward reinforcing steel.

Analysis of cement systems exposed to chloride showed that they react with the aluminate phases in the paste to form Friedel's salt: $3CaO{\cdot}Al_2O_3{\cdot}CaCl_2{\cdot}10H_2O$ [33–37]. This chloride bearing AF_m phase proved stable over a wide range of chloride concentrations [35,38]: from a few mmol/L to over 3 mol/L.

Other phases have also been identified in synthetic cement systems, such as the chloro-sulfate AF_m phase called Kuzel's salt ($3CaO{\cdot}Al_2O_3{\cdot}1/2CaCl_2{\cdot}1/2CaSO_4{\cdot}10H_2O$) [39]. Although no data could be found for the stability of Kuzel's salt in presence of alkalis, the solubility data given in reference [39] suggest that it only forms at low concentrations (<10 mmol/L).

Various forms of calcium oxychlorides have been reported by Brown and Bothe [35] The general composition of oxychloride compounds is $x Ca(OH)_2{\cdot}yCaCl_2{\cdot}zH_2O$. The compositions range from the simple 1:1:1 compound to more complex 4:1:10 or 3:1:12 assemblages. These chloride-bearing phases have mostly been observed in synthetic hydrated materials. But most importantly, oxychlorides observed in such laboratory conditions were only formed at very high chloride concentrations. For instance, the formation of the 3:1:12 phase requires approximately 4 mol/L of chloride while the 1:1:1 oxychloride is formed at a 9 mol/L chloride concentration [35]. In most practical cases, such as marine structures exposed to seawater or bridges and parking structures exposed to deicing salts, these concentration levels are not reached. It is thus doubtful that they form in structures unless chloride is concentrated by evaporation.

While many studies focused on the formation of Friedel's salt from hydrated C_3A systems, the role of Fe received very little attention. It is only recently that the formation of chloride-bearing minerals from hydrated C_4AF started has raised interest. Suryavanshi et al. [40] studied the binding of chloride in synthetic C_4AF hydrated with different levels of NaCl dissolved in the mix water. Chloride-bearing phases were identified using X-ray diffraction and differential scanning calorimetry. The results showed that a ferrite analogue to Friedel's salt was formed: $C_3F{\cdot}CaCl_2{\cdot}10H_2O$. This solid phase was also observed in reference [41] where pastes made of hydrated C_4AF and gypsum were exposed to a 10% NaCl solution over one-day wetting/drying cycles for durations between 28 and 56 days.

The previous paragraphs were concerned with the chemical interaction of chloride with hydrated cement paste. Chloride also physically interacts with the materials due to interaction at the pore solution/paste interface. In this case, new solid phases are not formed. Early binding experiments, such as the classical method devised by Luping and Nilsson [42], gave the overall amount of chloride that reacted with the material without making a distinction between physical and chemical interactions. But experiments with hydrated C_3S pastes (see for instance references [43–45]) or synthetic C–S–H [46]

evidenced this phenomenon, since the absence of C_3A or C_4AF in these materials prevents the formation of Friedel's salt.

3.2. Binding mechanisms

Many recent studies suggest that Friedel's salt formation is the result of chlorides reacting with hydrated phases such as monosulfates (SO_4–AF_m).

NMR results prompted Jones et al. [47] to propose two different mechanisms for Friedel's salt formation: dissolution/precipitation and ionic exchange. The authors argue that both mechanisms are taking place simultaneously, and that the relative importance of each one depends on the chloride concentration in the pore solution.

Many studies suggest that the main mechanism is ionic exchange. Suryanvanshi et al. [37] were among the first to raise this hypothesis, on the basis of pore solution analyses. They concluded that the positive principal layer of hydroxy-AFm C_4AH_{13} ($[Ca_2Al(OH^-)_6{\cdot}nH_2O]^+$) releases an OH^- ion in the pore solution and replaces it with a free Cl^-. The relationship between hydroxy-AFm and Friedel's salt was further studied by Birnin-Yauri and Glasser [38]. Their results showed an almost complete solid solution between the two phases. Only a small miscibility gap was identified. Munshi et al. [48] based their chloride binding model on a complete exchange mechanism between C_4AH_{13} and chloride ions in the pore solution:

$$[X-\mathrm{OH}]+\mathrm{Cl}^-\leftrightarrow[X-\mathrm{Cl}]+\mathrm{OH}^- \tag{30}$$

where X represents ion exchange sites.

Ionic exchange was also proposed between sulfate AF_m (monosulfate) and Friedel's salt [49]. In this case, the proposed reaction releases sulfate in the pore solution upon chloride binding:

$$[X-\mathrm{SO_4}]+2\mathrm{Cl}^-\leftrightarrow[X-\mathrm{Cl_2}]+\mathrm{SO_4^{2-}} \tag{31}$$

where X represents ion exchange sites.

As mentioned in the previous section, the other mechanism responsible for chloride binding is physical interaction. In a recent paper, Henocq et al. [44] modeled the interaction of ions in the pore solution with the surface of C–S–H using the double layer theory. The analysis showed that if a significant number of ions could be found in the diffuse layer, only a small fraction could be bound by specific adsorption. The model predictions were found to correlate quite well with experimental data. Overall, the authors found that physical binding could account for only a small fraction of all ions bound by the cement paste.

Hosokawa devised a model that combines the monosulfate-based ionic exchange mechanism presented previously with a physical interaction model [49]. As in the model developed by Henocq et al. [44], physical interaction is attributable to surface complexation and the electrostatic interaction of ions with the surface of C–S–H is also considered. Results also confirm that chemical reactions contribute much more than physical interaction to the total amount of chlorides bound by hydrated cement systems (Fig. 1).

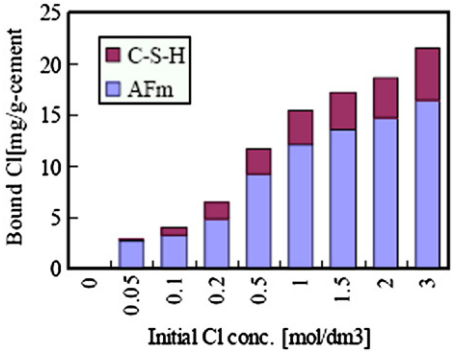

Fig. 1. Contribution of the chloride chemical binding with AFm and physical binding with C–S–H in a cement system (from Ref. [49]).

3.3. Modeling chloride ingress

As previously emphasized, early models, developed about 30 years ago, were based on a single mass transport equation solely limited to chloride transport. Under the following assumptions: negligible electrical coupling and chemical activity effects, constant temperature, saturated material, no complexation reactions in the pore solution, and a linear relationship between bound and free chloride, Eq. (8) can be simplified:

$$\frac{\partial C}{\partial t}-D_{\mathrm{app}}\frac{\partial^2 C}{\partial x^2}=0 \tag{32}$$

where C is the chloride concentration in solution and D_{app} is the apparent diffusion coefficient. This coefficient integrates both the diffusion characteristics of the material and the effect of chemistry on chloride penetration. It is important to note that according to the theory presented in Section 2, the parameter C represents the chloride concentration in the pore solution. An analytical solution of equation (32) is given by:

$$C=C_o\mathrm{erfc}\left(\frac{x}{\sqrt{4D_{\mathrm{app}}t}}\right) \tag{33}$$

where C_o is the chloride level at $x=0$. It should be emphasized that the validity of Eq. (33) rests on a series of simplifying assumptions (e.g. semi-infinite domain, constant D_{app} and constant exposure conditions) which are often not met in reality.

Eq. (33) has been used very loosely over the past decades. For instance, it has been noticed that measured chloride profiles have a shape similar to that of the profiles predicted by Eq. (32)). Experimental values have then been used to fit Eq. (33) and determine C_o and D_{app} (see for instance [50,51]). In addition to the questionable validity of Eq. (32), this approach is flawed considering that while the variable C appearing in the analytical solution corresponds to the concentration of ions in the pore fluid, the value of C_o accounts for both the chlorides bound to the paste and those found in solution.

Although this method is based on very shaky scientific foundations, it is still being used to estimate the service life of

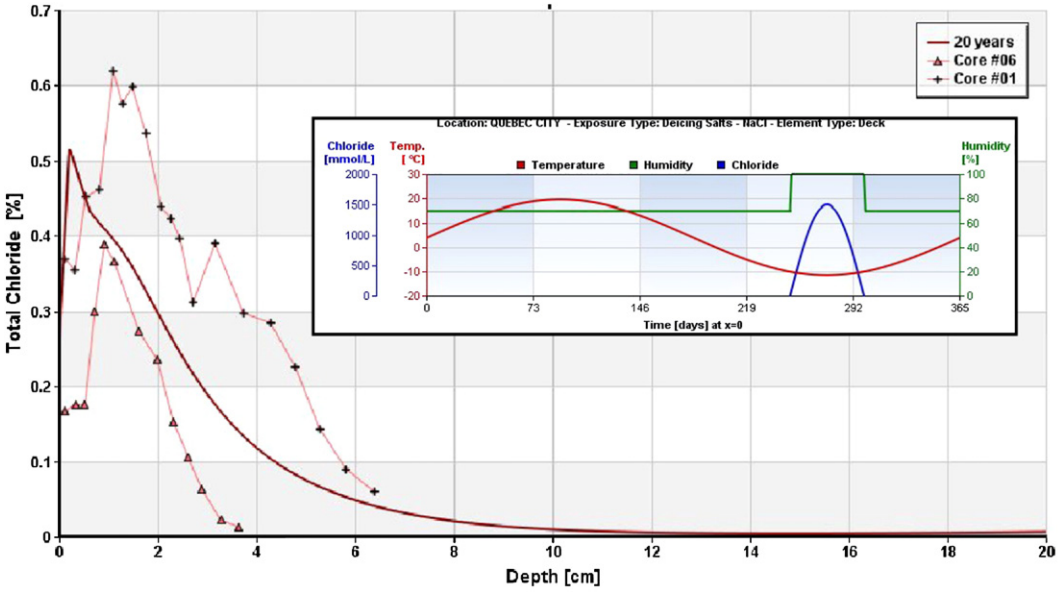

Fig. 2. Predicted total chloride profile in a 20-year-old parking structure using the model presented in Ref. [3], compared to measurements performed on two cores. The inserted graph illustrates the time-dependent boundary conditions over one year.

partially saturated structures exposed to chloride-laden environments. In an attempt to refine the analysis, some authors have relied to the isotherm method to describe chemical reactions [52]. According to this approach, the amount of bound chlorides is linked to the chloride concentration in solution by an empirical function similar to the curve shown on Fig. 1. This method does not allow a distinction between chemically and physically bound chlorides. By neglecting phenomena such as electrical coupling, chemical activity effects and Soret coupling, Eq. (8) becomes:

$$\rho \frac{\partial C^b}{\partial C}\frac{\partial C}{\partial t} + \frac{\partial (wC)}{\partial t} - \mathrm{div}(wD\mathrm{grad}(C) - VC) = 0 \qquad (34)$$

where C^b is the amount of bound chlorides and ρ is the density of the material. The term $\partial C^b/\partial C$ corresponds to the slope of the binding isotherm curve. This modeling approach as been used in references [19,32,53–55]. Eq. (34) can be coupled with the heat conduction Eq. (29) to take into account the effect of temperature [53]. It can also be combined with the moisture transport Eq. (24) or (26) to evaluate the moisture flux $\mathbf{V}$ and the water content [54,55]. Some authors also proposed models where Eq. (34) is coupled to both moisture and temperature diffusion equations [19,32].

While the previous approaches can be considered as improvements over Fick's second law of diffusion, they still neglect the interaction between the different ionic species present in solution. The current trend for ionic transport modeling focuses on multiionic approaches. For instance, models proposed by Masi et al. [30] and Truc et al. [29] consider that the transport of chlorides is coupled to that of other ionic species, using Eq. (8). In these papers, the electrochemical potential that couples the ionic species is solved using the nil current condition: $\sum_i z_i j_i = 0$. The chloride interaction with the paste is based on an interaction isotherm that does not consider the presence of other ionic species.

In the model presented by Samson and Marchand [3], chloride transport is based on the mass and energy conservation Eqs. (8), (24), (28) and (29)). The chemical interaction of chlorides with the hydrated cement paste is based on an ionic exchange mechanism between monosulfates and Friedel's salt as in Eq. (31). Typical simulation results are presented in Fig. 2. The predicted total chloride content accounts for chloride ions present in the pore solution and those found in Friedel's salts.

3.4. Prediction of corrosion initiation

Reinforcing steel corrosion is mainly induced by the ingress of chlorides upon exposure to marine environment or deicing salts [56]. Due to the high pH of the concrete pore solution, the steel surface is naturally passivated. However, this protective layer can be destroyed in the presence of chlorides. Corrosion is initiated when the chloride concentration at the vicinity of the steel surface reaches a critical value, called the chloride threshold. This chloride threshold is usually expressed as a ratio between the concentration of chlorides and that of hydroxyl ions ([Cl]/[OH]) or by the total amount of chloride in the material (wt.%) [57–59]. A comprehensive review of threshold values is presented in reference [57]. It shows a wide range of values depending on the characteristics of the mixture tested and on the test conditions. In most engineering analyses, the threshold value of 0.3% total chloride per cement weight (approximately 0.5 g of total chloride per kg of concrete) specified by the Federal Highway Administration (USA) [60] is used.

The time needed to reach the critical chloride content for corrosion corresponds to the initiation period [61]. It is determined

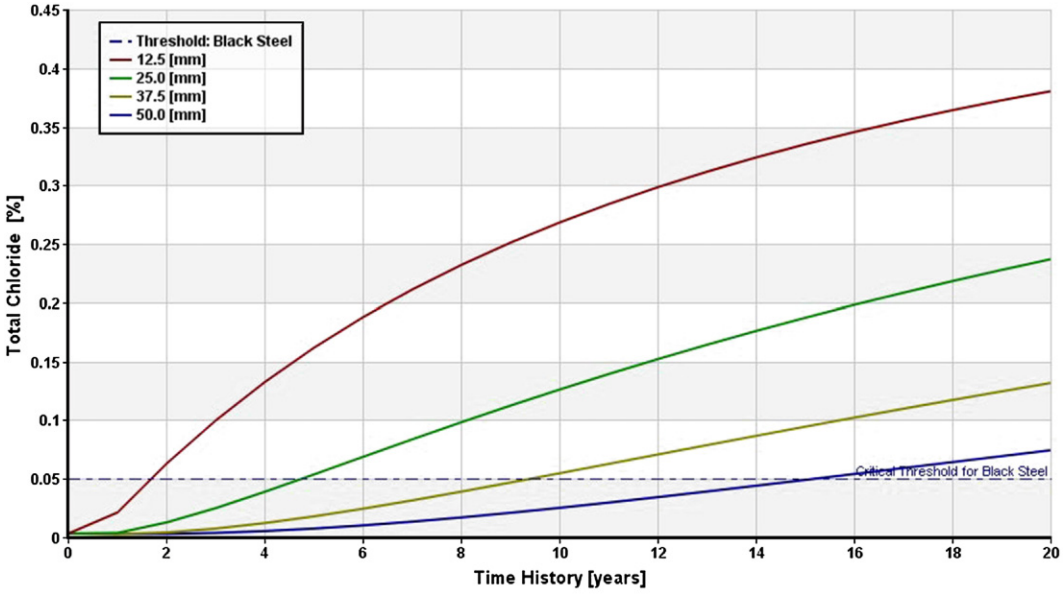

Fig. 3. Chloride content at different rebar positions (the calculations correspond to the case presented in Fig. 2).

by as series of parameters such as the properties of the concrete cover, its thickness and the exposure conditions. Modeling the penetration of chloride ions within cement-based materials using an advanced modeling approach (see the previous section) can thus provide a proper way of predicting corrosion initiation if a reliable threshold can be estimated. Fig. 3 illustrates a corrosion analysis based on the chloride ingress simulation showed in Fig. 2. It presents the time evolution of the total chloride content at various locations within the concrete element, thus allowing the determination of the initiation time.

4. Carbonation

The penetration of gaseous carbon dioxide within partially saturated concrete usually initiates a series of reactions with both ions dissolved in the pore solutions and the hydrated cement paste. The whole process can be summarized as a series of different steps. Gaseous carbon dioxide first penetrates the material. It then dissolves in the pore solution mainly as HCO_3^- and CO_3^{2-}. The CO_3^{2-} species then reacts with dissolved calcium to precipitate calcite, $CaCO_3$, as well as other CO_2-based solid phases. The pH drop associated with these reactions leads to the dissolution of portlandite. The early stages of carbonation, together with critical values for P_{CO2}, are given in reference [88].

The carbonation process itself does not have, *per se*, a negative effect on the paste properties. In some cases, it can even result in a reduction of the material porosity and favor formation of a protective layer at the surface of concrete. However, the drop in pH associated with the process can potentially have a detrimental effect on reinforced concrete structures by destroying the passive layer around rebars. The next sections summarize different aspects of the carbonation process.

4.1. Description of the carbonation process

When gaseous carbon dioxide is in contact with the pore solution of cementitious materials, it starts to dissolve as:

$$CO_{2(g)} \rightarrow CO_{2(aq)} \tag{35}$$

Under equilibrium conditions, the dissolution follows Henry's law, which is expressed in low (atmospheric) pressure environments as [63,64]:

$$\left(CO_{2(aq)}\right) = K_h P_{CO2} \tag{36}$$

where $(CO_{2(aq)})$ is the activity of the dissolved $CO_{2(aq)}$, K_h is Henry's constant and P_{CO2} is the partial pressure of $CO_{2(g)}$ in the gas phase. The temperature-dependent value of K_h can be expressed as [63]:

$$\log K_h = 108.3865 + 0.01985076T - 6919.53/T - 40.45154 \log T + 669365.0T^2 \tag{37}$$

where T is the temperature.

Once in solution, $CO_{2(aq)}$ dissociates into different ionic species according to the following reactions:

$$CO_{2(aq)} + H_2O \rightarrow H^+ + HCO_3^- \tag{38}$$

$$HCO_3^- \rightarrow H^+ + CO_3^{2-} \tag{39}$$

These reactions respectively obey the following equilibrium relationships:

$$K_1 = (H^+)(HCO_3^-)/(CO_{2(aq)}) \tag{40}$$

$$K_2 = (H^+)(CO_3^{2-})/(HCO_3^-) \tag{41}$$

where the parentheses (…) indicate chemical activity. The time-dependent values for K_1 and K_2 are given in reference [63].

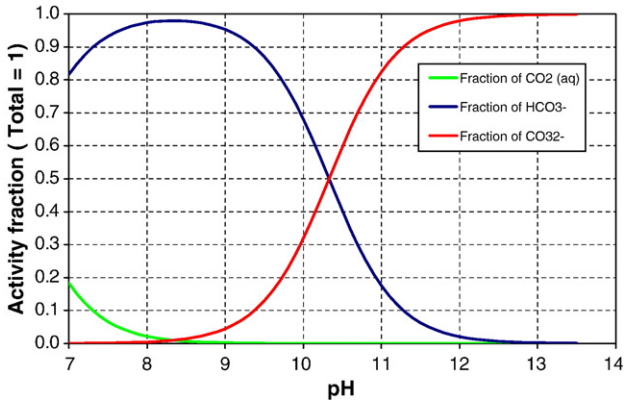

Fig. 4. Relative distribution of $CO_{2(aq)}$, HCO_3 and CO_3^{2-} as a function of pH at 25 °C.

Using Eqs. (40) and (41) with the water dissociation relationship:

$$(H^+)(OH^-) = 10^{-14} \quad (42)$$

it is possible to estimate the fraction of each ionic species in solution as a function of the pH. This is illustrated by Fig. 4. It shows that in cementitious materials, where pH values are usually high, the dominant species in solution is CO_3^{2-}. Barret et al. [65] suggested that reactions (37), (38) and (41) could be summarized by:

$$CO_{2(aq)} + OH^- \rightarrow CO_3^{2-} + H_2O \quad (43)$$

This reaction illustrates that carbonation lowers pH by consuming hydroxide ions and producing water.

Once CO_3^{2-} is in the pore solution, it is free to react with other ionic species to precipitate carbonate phases. While aragonite and valerite polymorphs of $CaCO_3$ have been reported, calcite ($CaCO_3$) is generally identified as the main reaction product of carbonation [66,67]. It precipitates according to the reaction:

$$Ca^{2+}_{(aq)} + CO_3^{2-} \rightarrow CaCO_{3(s)} \quad (44)$$

where the solubility constant has a value of $\log(K) = -8.48$ at 25 °C [63]. The presence of carbonates in solution can also lead to the formation of other solid phases. Barret et al. [65] studied carbonation reactions by considering the formation of calcium hydrocarboaluminate $3CaO{\cdot}Al_2O_3{\cdot}CaCO_3{\cdot}11H_2O$. The thermodynamic equilibrium of similar solid phases is described in references [68–70].

According to Eqs. (43) and (44), the different mechanisms leading to the formation of calcite reduce the amount of calcium and hydroxide ions in the pore solution, which in turn triggers the dissolution of portlandite. The formation of calcite in replacement of portlandite reduces the porosity of the material since calcite has a higher molar volume (36.9 cm^3/mol compared to 33.1 cm^3/mol for CH). Experimental evidence of calcium hydroxide reduction upon calcite formation was recently reported [71,72].

4.2. Carbonation measurements

Carbonation depth is traditionally estimated using a phenolphthalein indicator. This in an indirect measure since the pink indicator actually shows where the pH drops below 9 by de-colorizing. Fig. 5a presents mortar samples made at different water to cement ratios sprayed with phenolphthalein after 14 and 28 days of exposure to a 50% RH 5% CO_2 environment. Fig. 5b shows that a plot of carbonation depths measured with phenolphthalein versus the square root of time yields a linear relationship. This is a common feature of the carbonation process (see for instance Ref. [66]).

However, recent measurements showed that this technique only gives an approximate estimation of the depth of carbonation. Using a technique similar to the acid-dissolution approach for chloride profile measurements, Houst and Wittmann [73] measured carbonate profiles in mortars exposed for 40 months to an outdoor environment. Results show that the carbonate profiles extend well beyond the depth indicated by phenolphthalein.

Similar measurements were reported by Baroghel–Bouny and Chaussadent [74]. Calcite profiles were measured in paste samples maintained in an accelerated carbonation room.

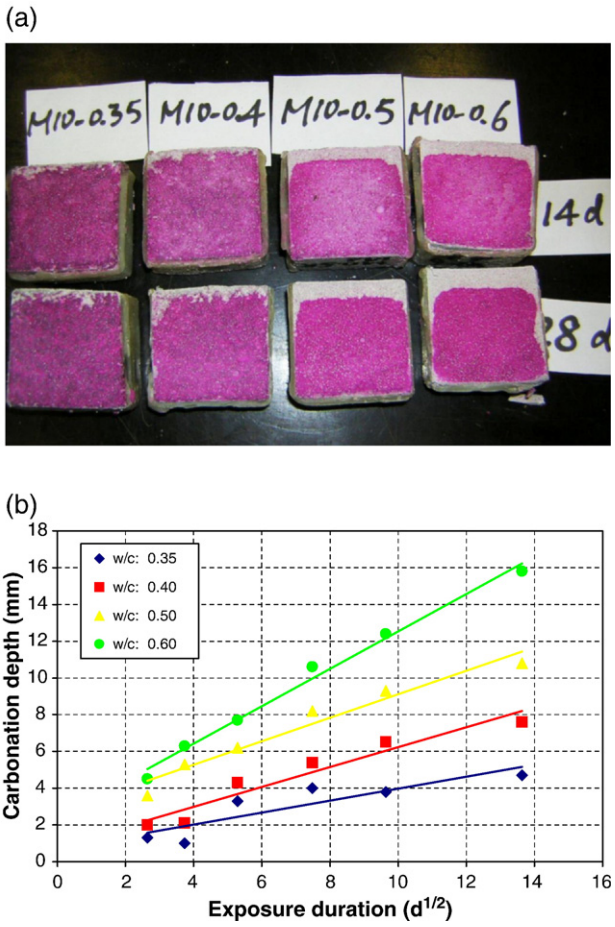

Fig. 5. a — Carbonation depths measured with phenolphthalein on various mortar samples exposed to a 50% RH 5% CO_2 environment. b — Carbonation depths plotted against the square root of time. (Data provided by the author).

Portlandite profiles were also determined. Results show a drop of portlandite near the exposed surface, where the calcite content reaches its maximum value. According to these measurements, residual calcium hydroxide is still present near the solid/environment interface even though the material is carbonated.

4.3. Carbonation models

Numerous models dedicated to the prediction of the depth of carbonation can be found in the literature [67,75–78]. In all cases, the ingress of $CO_{2(g)}$ in the material is modeled using a diffusion-based equation:

$$\frac{\partial(\phi - w)\left[CO_{2(g)}\right]}{\partial t} - \mathrm{div}\left((\phi - w)D_c \mathrm{grad}\left[CO_{2(g)}\right]\right) - f_c = 0 \quad (45)$$

where ϕ is the porosity of the material, w is the volumetric water content, $[CO_{2(g)}]$ is the gaseous carbon dioxide concentration, D_c is the gas diffusion coefficient and f_c is a sink term. In the models proposed in references [67,75,77,78], the parameter D_c is a function of the local water content in the material. In the approaches proposed by [67,77,78] the effect of temperature on gas transport is also considered. In Eq. (45), the sink term f_c accounts for the transfer of carbon dioxide from the gaseous phase to the pore solution of the material [see Eq. (35)].

Since gaseous carbon dioxide must enter the material to initiate the carbonation process, it is necessary to model the drying process. The models cited previously are all based on Richards' equation (23) or its relative humidity counterpart (26)). In references [77,78], a source/sink term is added to Eq. (26) to model the hydration of the cement paste. This source/sink term in [77] also accounts for the formation of water involved in the carbonation process [see Eq. (42)].

Based on Eqs. (45) and (24), it is possible to evaluate the amount of carbon dioxide in the pore solution $CO_{2(aq)}$, and consequently the extent of the carbonation process. In most models, the reactions described in Section 4.1 are summarized as [76,77]:

$$Ca(OH)_{2(s)} + CO_{2(aq)} \rightarrow CaCO_{3(s)} + H_2O \quad (46)$$

Simple rate equations are then used to calculate the formation of calcite or the loss of portlandite, such as [67]:

$$\frac{d\left[CaCO_{3(s)}\right]}{dt} = f\left(w, T, \left[Ca(OH)_{2(s)}\right], \left[CO_{2(aq)}\right]\right) \quad (47)$$

In reference [75], the concentration of Ca^{2+} in solution is also taken into account, using an equation similar to Eq. (45). The source term represents the calcium that dissolves in solution when portlandite and C–S–H dissolve: it is assumed that $CO_{2(g)}$ dissolves in the pore solution as CO_3^{2-}. The amount of CO_3^{2-} in solution can be calculated from the source term in Eq. (44), but the transport of this ionic species in solution is neglected. Calcite is formed according to the equilibrium relationship:

$$[Ca^{2+}][CO_3^{2-}] = 10^{-8.35} \quad (48)$$

where the square brackets […] indicate concentrations. Calculations do not consider the presence of alkalis, since Ca^{2+} varies between 22 mmol/L (when portlandite is still present) to <1 mmol/L (upon complete decalcification of the C–S–H). In Ref. [78], the formation of calcite is modeled according to:

$$\frac{d\left[CaCO_{3(s)}\right]}{dt} = k_r\left[Ca^{2+}\right]\left[CO_3^{2-}\right] \quad (49)$$

where k_r is a reaction rate. The concentration of CO_3^{2-} follows Henry's law. The concentration of Ca^{2+} in the pore solution is calculated from a series of chemical equilibrium relationships. As in reference [75], the movement of these species is not considered in the model, nor is the presence of alkalis.

This short review emphasizes the main shortcomings of most carbonation models. In most cases, the prediction of the pH drop is not part of the model since OH^- concentration is neglected. This is particularly detrimental when the risk of corrosion needs to be evaluated. Also, one of the main characteristic of cementitious materials, which is the highly alkaline pore solution, is neglected. From the chemical point of view, the presence of high Na^+ and K^+ concentrations are likely to significantly influence the carbonation process.

4.4. Relationship with chloride ingress

Recent studies suggest that chloride binding and carbonation are intimately related [136]. In presence of $CO_{2(g)}$, Friedel's salt, the main solid phase formed from the reaction between chloride and an hydrated cement paste (see Section 3.1), tends to react. This reaction liberates Cl^- ions to the pore solution. Depending on the concentration gradients in the material, chloride thus liberated may reach the rebar and initiate corrosion.

5. Decalcification

The decalcification process is usually described by the dissolution of portlandite and C–S–H in hydrated cement systems exposed to pure water, even though dissolution can be observed in other environments such as seawater. The leaching of ions (mainly calcium and hydroxide) from the pore solution to the external environment is responsible for the dissolution of these hydrates. This phenomenon typically affects structures which have been in contact with pure and acidic waters for long periods: dams, water pipes, radioactive waste disposal facilities, etc. Over the past two decades, it has been identified as a very relevant issue for nuclear waste storage. The chemistry of attack has been described by Dow and Glasser [62]. It is shown how regimes of passivation and attack can be distinguished. The consequences of ionic leaching are an increase of the porosity and permeability, and a loss of mechanical strength.

5.1. Experiments and methods

Different test methods were developed to perform concrete decalcification experiments. Immersion tests in water

(deionized or mineralized) are mainly used for characterizing the leaching process [80–83]. In some studies, tests were performed on ground material to measure the amount of leached calcium [84,85].

Since calcium leaching is a relatively slow process, a wide range of accelerated tests have been developed. The majority of these procedures are carried out with strongly acidified solutions (like ammonium nitrate) instead of deionized water [86–88]. In some cases, authors have also relied on organic acids to accelerate the leaching process [89]. Finally, in some others, calcium leaching was accelerated by applying an electrical potential gradient across a specimen [53,90].

5.2. Description of the process

The leaching of calcium is a coupled dissolution/diffusion process. Leaching by deionized water induces calcium and hydroxide concentration gradients which continuously decrease from the sound zone to the exposed surface of the material. This causes the diffusion of calcium and hydroxide ions from the pore solution to the aggressive solution, and thus lowers the amount of calcium concentration in the pore solution. Loss of calcium leads to the dissolution of portlandite and secondary precipitations of AF_m, ettringite and calcite [91,92]. The precipitation of these minerals takes place in the innermost part of the degraded zone while they are dissolved in the outermost part of the altered zone [91,92]. But overall, the process mainly leads to the dissolution of calcium hydroxide and the decalcification of C–S–H [81,91,93].

The altered material can be seen as a layered system composed of [93]:

- An unaltered core delineated by total dissolution of portlandite,
- Different zones separated by dissolution or precipitation fronts (AFm, AFt,...),
- Progressive decalcification of C–S–H.

The degraded zone induced by water exposure is characterized by a decalcification of C–S–H inducing a silicate polymerization. The Ca/Si ratio of the C–S–H gradually decreases between sound and leached zone. Moreover, trivalent iron and aluminum from dissolved phases like AF_m and ettringite are incorporated into the C–S–H [80,84,91,92].

Cement hydrates in contact with water are dissolved depending on their solubility properties. According to their respective solubilities, hydrates dissolve successively in order to restore the chemical equilibrium between pore solution and crystallized hydrates. Properties of cement hydrates dissolution were characterized by Berner [94] and Reardon [7] and new data, including hydrogarnet, siliceous hydrogarnet and strätlingite (C_2ASH_8) are presented by Matschei, Lothenbach and Glasser [88]. The solubilities of the main hydrated phases are classified in the following order: $SC_{a(OH)2} > S_{Afm} > S_{friedel's\ salt} > S_{Aft}$ [103,126]. The kinetics is influenced by the composition of the aggressive solution (CO_2, mineralized...) [83,95–97] or by the saturation of the specimens [83].

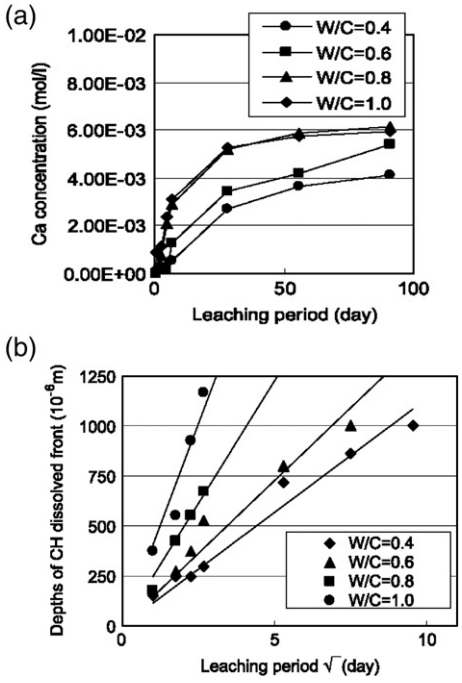

Fig. 6. Change of Ca^{2+} concentration with the leaching period (a) and depth of the $Ca(OH)_2$ dissolved front as a function of the square root of the leaching period (b) [81].

As mentioned previously, calcium hydroxide is the main phase affected by the exposure to water. Calcium hydroxide depletion increases with the exposure period [81,82,85,90,98]. Fig. 6 shows the influence of the water-to-cement ratio on the dissolution kinetics. The amount of leached calcium increases with water-to-cement ratio [81,90]. A higher w/c value corresponds to a higher porosity (higher permeability and higher pore volume) and a higher initial portlandite content [81,96].

The increasing calcium concentration in solution is associated to a gradual penetration of the $Ca(OH)_2$ dissolution front (Fig. 6(b)). The depth of penetration increases with water-to-cement ratio, which correlates with the results given in Fig. 6(a) [81].

Decalcification changes the bulk density and the pore structure of the hydrated cement paste. Haga et al. showed that the increase of pore volume is larger for a higher initial amount of $Ca(OH)_2$ [81]. This increase of pore volume is attributable to the dissolution of $Ca(OH)_2$ while the porosity created by C–S–H decalcification is negligible (Fig. 7) [81,82,86].

The use of supplementary cementing materials, combined with adequate curing, decreases the permeability of concrete and changes the kinetics of calcium leaching. Fig. 8 shows the influence of blast-furnace slag and silica fume on calcium leaching [90]. The beneficial influence of both supplementary cementing materials is due to the reduction in the initial portlandite content (resulting from the pozzolanic reaction) and to a significant reduction of the transport properties of the mixtures [90,96].

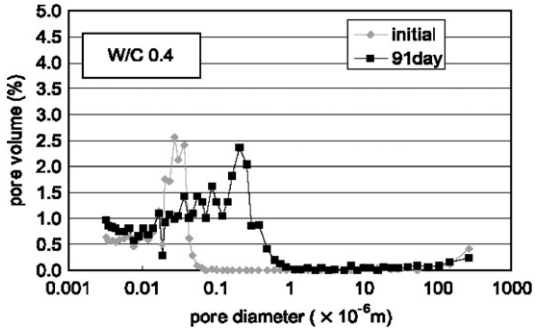

Fig. 7. Pore size distribution of the initial sample and that leached for 91 days [81].

The pore volume increase resulting from calcium leaching has a detrimental influence on the mechanical properties of cement-based materials. The relationship between pore volume and strength for sound and altered mortars was clearly shown by Saito and Deguchi (Fig. 9(a)) [90]. Uniaxial compression tests on leached materials were performed by Carde et al. [86]. The total leaching of portlandite and the progressive decalcification of C–S–H led to a linear dependence of the strength on the ratio A_d/A_t between the degraded (A_d) and the sound (A_t) cross-sections (Fig. 9(b)) [86,87]. The results shown on Fig. 9 confirm the improvement of the leaching resistance associated with the use of supplementary cementing materials.

5.3. Modeling the decalcification process

The calcium leaching in cement-based materials is a coupled chemical equilibrium/diffusion phenomenon. The kinetics and the mechanisms of this ionic transport process are described by

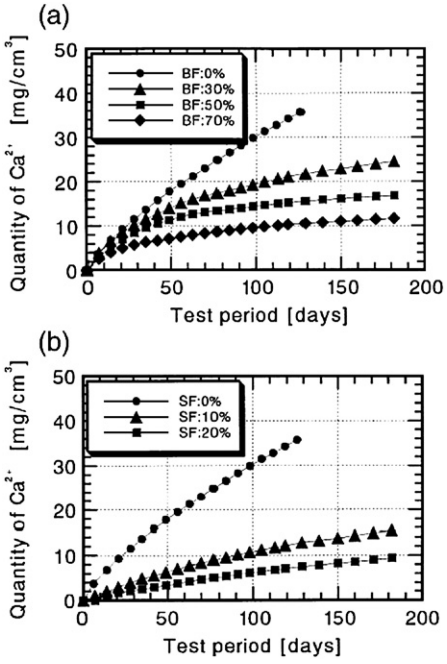

Fig. 8. Cumulative quantity of dissolved Ca^{2+} for SCM mixtures: (a) blast-furnace slag (BF) and (b) silica fume (SF) [90].

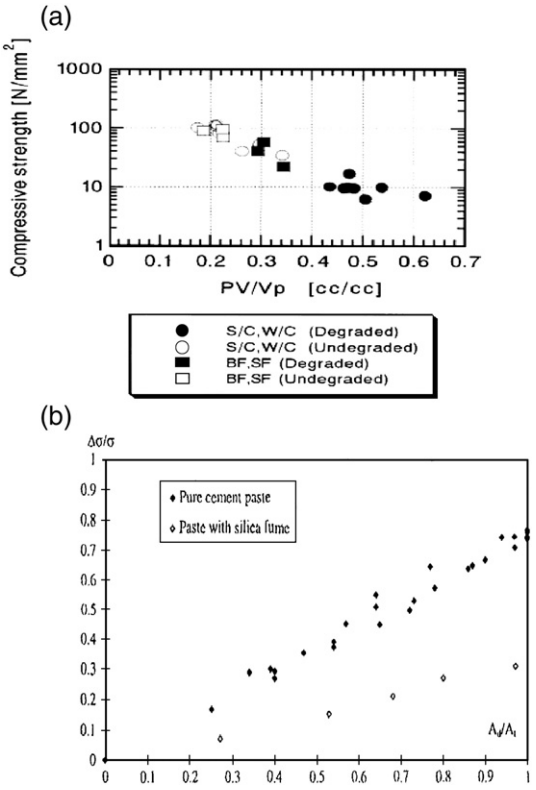

Fig. 9. (a) Relationship between porosity (PV/Vp) and compressive strength for sound and degraded materials [9] and (b) variation of the strength loss in relation to the degradation ratio A_d/A_t [86].

Eq. (8). Most models found in the literature are based on a simplified version of Eq. (8) [81,82,85,99]:

$$\phi(x,t)\frac{\partial C(x,t)}{\partial t} = D(x,t)\frac{\partial^2 C(x,t)}{\partial x^2} - \frac{\partial C_s(x,t)}{\partial t} \tag{50}$$

where $C(x,t)$ is the Ca^{2+} concentration in the liquid phase, $C_S(x,t)$ is the content of Ca in solid phase, $\phi(x,t)$ is the porosity and $D(x,t)$ is the effective diffusion coefficient of Ca^{2+} ions. In Eq. (50), the influence of phenomena such as chemical activity, convection and electrical coupling is neglected. The calcium content in solid $C_S(x,t)$ is calculated from its relationship with calcium concentration in solution (Fig. 10) [81,82,85].

Another approach consists in determining the calcium content in solid by solving the chemical equilibrium between the minerals and the pore solution. The modeling of calcium leaching of hardened cement pastes in deionized water, by coupling Eq. (8) and the dissolution/precipitation equilibrium of $Ca(OH)_2$ and C–S–H, was presented by Maltais et al. [83]. The dissolution of portlandite and the decalcification of C–S–H were defined by their solubility constants $K_{Ca(OH)2}$ and K_{CSH} respectively (Table 1).

The different leaching models take into account the evolution of the porosity of the material as solid phases dissolve. This increase of porosity as calcium is leached is given by [81,83,85,99]:

$$\phi_{\text{leaching}} = \frac{M_{Ca(OH)_2}}{d_{Ca(OH)_2}}\left(C_{S,Ca(OH)_2}{}^{0} - C_{S,Ca(OH)_2}\right) \tag{51}$$

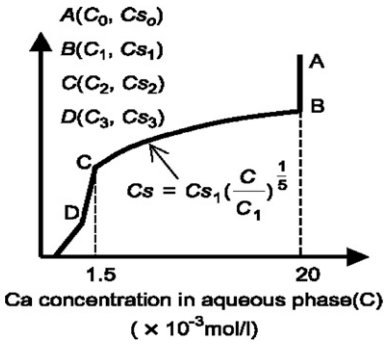

Fig. 10. Relationship between Ca concentrations in the solution and the solid from Daimon et al. [81,100].

This pore volume increase modifies the diffusion coefficient of calcium. Most empirical relationships linking the diffusion coefficient to porosity are similar to Eqs. (17) and (18). Others relationships are presented in Table 2.

Marchand et al. [102] proposed a direct relationship between a normalized diffusion coefficient D_N and the fraction of $Ca(OH)_2$ (CH) leached:

$$D_N = 1 + \frac{1.1 \cdot CH^2}{0.28 + 0.79 \cdot CH} \quad (52)$$

where D_N is defined as: $D_N = 1 + \frac{D(CH) - D(CH=0)}{D(CH=100) - D(CH=0)}$.

Fig. 11 presents simulations results compared to experimental data [83,85]. The results in Fig. 11(a) are obtained by solving Eq. (8) coupled with chemical equilibrium while results in Fig. 11(b) are determined by solving Eq. (50) coupled with the calcium in solid phase relationship given by Fig. 10.

6. Sulfate attack

Cement-based materials exposed to sulfate-bearing solutions such as some natural or polluted ground waters (external sulfate attack), or by the action of sulfates present in the original mix (internal sulfate attack) [97,103] can show signs of deterioration. Sulfate ions react with ionic species of the pore solution to precipitate gypsum ($CaSO_4.2H_2O$), ettringite ($[Ca_3Al(OH)_6 \cdot 12H_2O]_2 \cdot (SO4)_3 \cdot 2H_2O$) or thaumasite ($Ca3[Si(OH)6 \cdot 12H_2O] \cdot (CO_3) \cdot SO_4$) [97] or mixtures of these phases. The precipitation of these solid phases can lead to strain within the material, inducing expansion, strength loss, spalling and severe degradation.

This section focuses on cementitious materials exposed to external sulfate sources only.

Table 1
Solubility constants of portlandite and C–S–H [83,94]

Name	Chemical composition	Expression for equilibrium (K_{sp})	$-\log K_{sp}$
Portlandite	$Ca(OH)^2$	$\{Ca^{2+}\}\{OH^-\}^2$	5.2
C–S–H (Maltais04)	0.65 Ca $(OH)_2$ + CaH_2SiO_4	$\{Ca^{2+}\}\{OH^-\}^2$	6.2
C–S–H (Berner92, Henocq07)	CaH_2SiO_4 or $5CaO \cdot 5SiO_2 \cdot 10.5H_2O$	$\{Ca^{2+}\}\{H_2SiO_4^{2-}\}$ or $\{Ca^{2+}\}^5 \cdot \{H_3SiO_4^-\}^6 \cdot \{OH\}^4/\{H_2O\}^{0.5}$	$f(C/S)$ [a]

[a] $-\log Ksp$ is a function of C/S ratio according to the empirical function f.

Table 2
$D=M(\phi)$ relationships found in literature

$D=M(\phi)$ relationship	Reference
$D=e^{(9.95\phi-29.08)}$	[82]
$D=(\varphi(x,t)/\phi_0)^n D_0$	[81]
$D=(0.001+0.07\phi^2+H(\phi-\phi_c)1.8(\phi-\phi_c)^2)D_0$	[101]
$D=\frac{1-cG_{vol}}{1-dS_{vol}} P_{vol} f(\phi-\phi_{gel}) D_0$	[102]

6.1. Description of the sulfate attack process

The ingress of sulfate ions into cementitious materials from Na_2SO_4 or K_2SO_4 sulfate-bearing solutions is generally coupled with calcium leaching since groundwater are usually near the neutral state (pH ≈ 7). Depending on the conditions, it may lead to the formation of gypsum in a layer close to the exposed surface in which calcium hydroxide is leached and/or reacted, C–S–H are decalcified. Also, ettringite forms from monosulfate in a zone

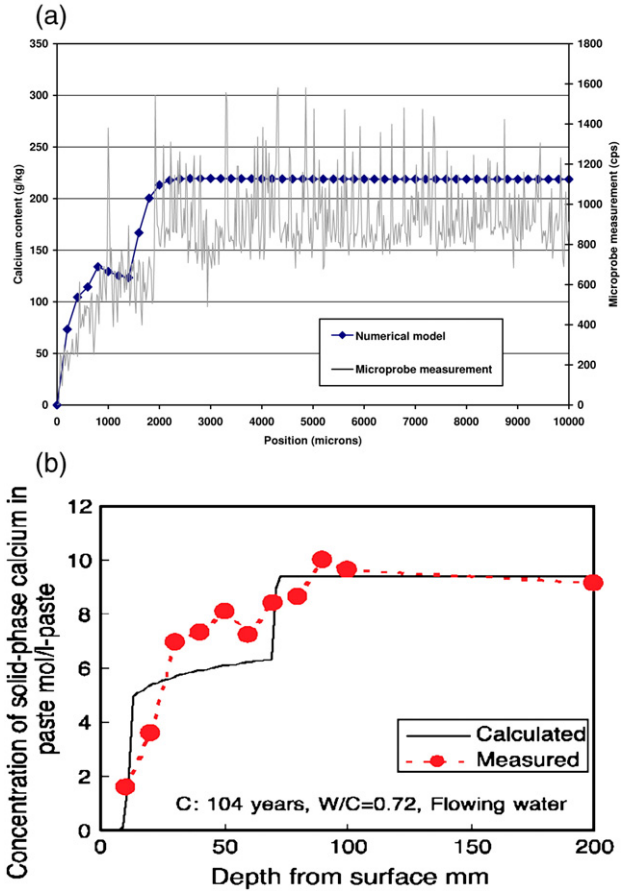

Fig. 11. Simulations of calcium leaching: (a) on cement paste [83] and (b) on mortar [85].

where calcium hydroxide is reduced [34,79,83,103,104]. In the presence of magnesium, the mechanism of sulfate ingress is different. In this case, the penetration of sulfate and magnesium ions is mainly characterized by the formation of brucite ($Mg(OH)_2$), an M–A–H phase resembling hydrotalcite and a M–S–H gel. These replace C–S–H in addition to gypsum and ettringite formation. Particularly, the formation of M–S–H from C–S–H can result in more expansion and thus more degradation [79,103,105].

The formation of gypsum and ettringite may lead to expansion and ultimately cracking. The formation of ettringite is often considered as the predominant cause of volume instability of hydrated cement systems in presence of sulfate solutions [103,116]. However, formation of gypsum was shown to cause expansion of C_3S hydrated pastes and can probably contribute to the degradation of concrete in sulfate-laden environments [107].

Sulfate attack cannot occur in isolation: sulfate is always balanced by cations, whose presence cannot be ignored. For example, protons associated with sulfate give sulfuric acid which attacks cement paste (and certain aggregates) strongly. The proton dissolves calcium and, to a lesser extent, alumina. As the acidity is reduced by reaction, gypsum and ettringite develop leading to expansion and loss of coherence. Other cations, such as sodium and potassium, do not form insoluble phases but influence the aqueous pH and interact strongly with carbon dioxide, if present. Calcium and magnesium, particularly the latter, alter the course of reaction by forming insoluble phases; for example Mg forms brucite, $Mg(OH)_2$ as well as hydrotalcite like phases and/or a poorly-crystalline magnesium silicate hydrate. The inability to separate cation and anion reaction means that attack takes many forms, given the complex geochemistry of natural sulfate-containing waters.

Many factors can influence the degradation of concrete by sulfate attack [108]. Water-to-cement ratio, for instance, has been found to have a significant effect on both the penetration of sulfate ions and the resulting expansion (Fig. 12) [103,106,108,109]. This is the reason why many standards limit the maximum water-to-cement ratio of concrete structures exposed to sulfates.

The concentration of the sodium sulfate also influences the ratio of gypsum and ettringite. Matschei and Glasser [110] show that the ettringite is predominant at low sodium sulfate concentrations, *ca* 3 g/l, but as the concentration of the test solution is increased to *ca* 30 g/l, gypsum increasingly predominates. Calculations of the volume change attending reaction, corrected for dissolution, disclose that gypsum formation contributes significantly to the total expansion but that the overall contribution increases as the concentration of sodium sulfate is increased.

The mineralogy of cement, especially its C_3A content and total aluminate content, is also known to influence the mechanisms of degradation. Expansion has been found to increase with the C_3A content (Fig. 13) [103,106,108,111], which directly influences the amount of AF_m in the hydrated cement paste which reacts with sulfate ions to form ettringite.

In many practical cases, leaching also occurs. This loss of matter tends to counteract the volume increase associated with ettringite formation. For example, sulfate attack in sea water is limited by the enhanced dissolution of $Ca(OH)_2$, which is typically solubilized by chlorides.

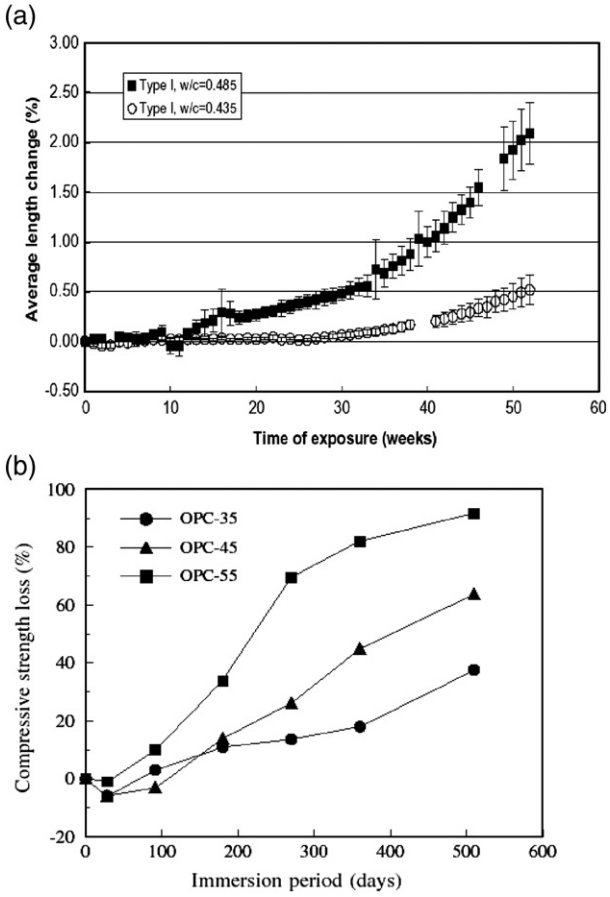

Fig. 12. Expansions of mortars under sodium sulfate attack as a function of W/C: (a) [106] and (b) [109].

As expected, concrete mixtures prepared with supplementary cementing materials show a better resistance to sulfate attack by reducing their permeability [105,108,109,112]. Metakaolin replacement [113], silica fume [109], slag [105,112] and fly ash [108] reduce the expansion of specimens undergoing sulfate attack. However, the ability of supplementary cementing materials to limit damage is much less significant in the presence of $MgSO_4$ (Fig. 14) [105].

The presence of sulfate ions can also lead to the formation of thaumasite. Such a phenomenon occurs when the following conditions are present: SO_4^{2-}, C–S–H, CO_3^{2-} and water [97,114,115]. Numerous cases of field concrete degradation associated with thaumasite formation have been reported for structures exposed to relatively low temperatures. This led some authors to believe that thaumasite was only stable at temperatures lower than ~10 °C. However, its formation, while kinetically slowed by rising temperature, is feasible to at least to 30 °C: unpublished data by one of the authors (FPG) put the limit of thermal stability of thaumasite at ~45 °C. Higher temperatures, around 20 °C have been reported. Unexpected thaumasite was noted in warm climates such as California [116], Switzerland [117] and Italy [118]. Clearly, thaumasite forms

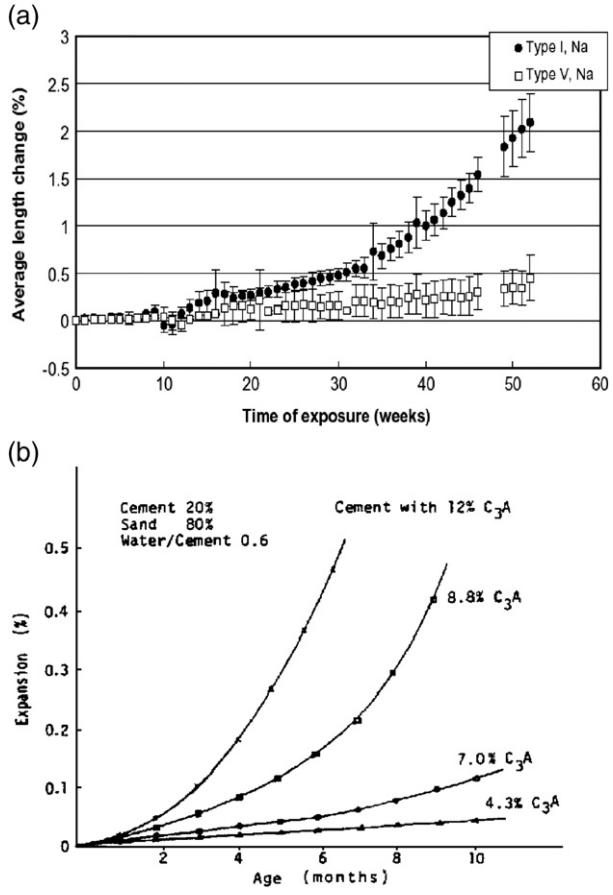

Fig. 13. Expansions of mortars under sodium sulfate attack as a function of C_3A content: (a) $\%C_3A_{typeI} > \%C_3A_{typeV}$ [106] and (b) [108].

readily at low temperature but cold temperatures are not an essential criterion [119].

The influence of temperature on carbon dioxide solubility is a possible reason why thaumasite forms more readily at 5 °C [119]. Moreover, Collet et al. assume that calcium bicarbonate, instead of calcium carbonate, would be the source of carbonate ions required for thaumasite formation [119]. C–S–H provide the source of silicate ions which react to form thaumasite. Thaumasite, which apparently has no capacity to act as a binder, gradually replaces C–S–H explaining why cementitious materials can be severely degraded by its formation [97,103,115,120].

Two mechanisms have been proposed to describe the formation of thaumasite:

- Thaumasite forms from ettringite by substitution of Al^{3+} by Si^{4+} in the presence of CO_3^{2-} [114,121,122,137],
- Thaumasite is the result of the direct interaction between C–S–H, sulfates and carbonates [120–122].

Thaumasite, when produced from ettringite and C–S–H mixtures is not a pure mineral and contains other cations and anions in solid solution [114]. More likely, thaumasite forms according to a through-solution process. As proposed by Crammond [115], ettringite can serve as a template for the initial nucleation of thaumasite. However, additional precipitation arises from solution. That would explain why some alumina is apparently beneficial [103,115]. Overall, the ability of cements to allow thaumasite formation is said to be proportional to their C_3A or Al_2O_3 contents [122].

Thaumasite formation is delayed in the case of concrete mixtures prepared with supplementary cementing materials. Influence varies with the type and the source of materials. Metakaolin and slag have been found to improve the behavior of limestone cements. However, mixtures prepared with fly ash remain vulnerable to thaumasite sulfate attack (Fig. 15) [123]. The use of fly ash simply seems to retard sulfate attack [124]. Moreover, supplementary cementing materials offer an effective resistance if they react sufficiently quickly [124]. That explains why « sulfate resistant » Portland cement does not give an improvement of resistance against thaumasite formation [103,123].

6.2. Experiments and methods

Various experimental approaches have been used to investigate the performance of hydrated cement systems exposed to sulfate solutions. Santhanam et al. have reviewed and criticized the different test methods proposed in the literature. Their analysis clearly emphasized the significant influence of experimental conditions [such as the control of pH, sulfate concentration and type of salts (Na_2SO_4, $MgSO_4$, H_2SO_4…)] on the performance of test specimens [120]. Immersion tests in large volume or with renewed solutions are commonly used to maintain constant test conditions [83,107,125].

Microstructural alterations resulting from the exposure to sulfate-bearing solutions can be subsequently analyzed using different techniques such as microprobe analyses [83], SEM, EDS and/or XRD for identifying crystallized phases [34,107]. Naik et al. have also relied on X-ray microtomography and spatially resolved energy dispersive X-ray diffraction (EDXRD) to monitor the behavior of specimens exposed to sulfate solutions [106]. In some cases, damage induced by the exposure to sulfates can also be determined by compressive strength and/or volume change measurements [105,106,108,112].

Most test methods used to investigate the resistance of cement systems to thaumasite formation are typically performed at around 5 °C [119,124–127]. However, some authors have also elected to investigate the influence of thaumasite by running tests at 20 °C [123,124,128,138]. Otherwise, thaumasite formation is mainly studied on field samples from different exposure conditions [115–117,129–131]. As thaumasite precipitation can occur in various environments, its solubility and its stability was respectively investigated from solid solutions by Macphee et al. [132] and in cement pastes by Juel et al. [133]; further data are in the course of preparation by the author (FPG).

6.3. External sulfate attack modeling

Empirical, mechanistic and numerical models are proposed in literature for predicting the behavior of cement systems

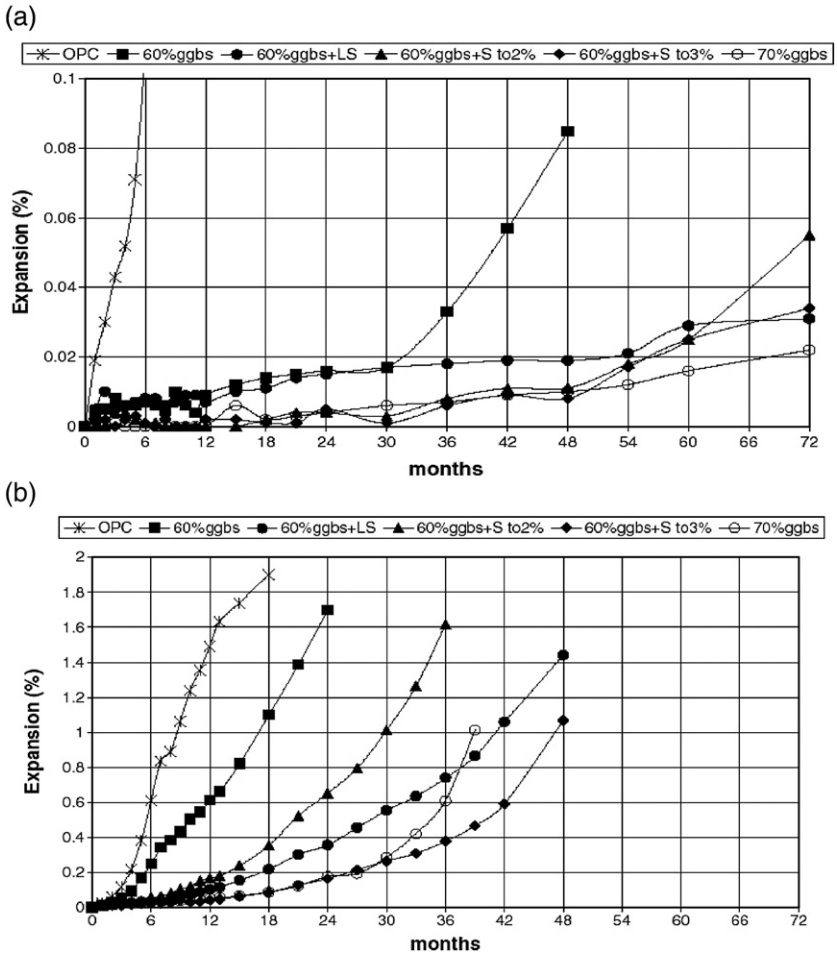

Fig. 14. Expansions of Sandberg prisms for different slag content: (a) in Na2SO4 solution (1.5% SO_3) and (b) in $MgSO_4$ solution (1.5% SO_3) [105].

exposed to sulfate-laden environments. Empirical models estimate the sulfate resistance factor [114], the expansion under sulfate attack [103,134] or the location of the visible degradation zone [103]. Mechanistic models typically attempt to take into account the mechanisms leading to the deterioration of the material. These models usually predict the rate of sulfate attack and the fractional or volumetric expansion [103]. Ionic transport models simulate the chemical reactions occurring during sulfate attack and, in some cases, also estimate the damage caused by expansion [83,103,135].

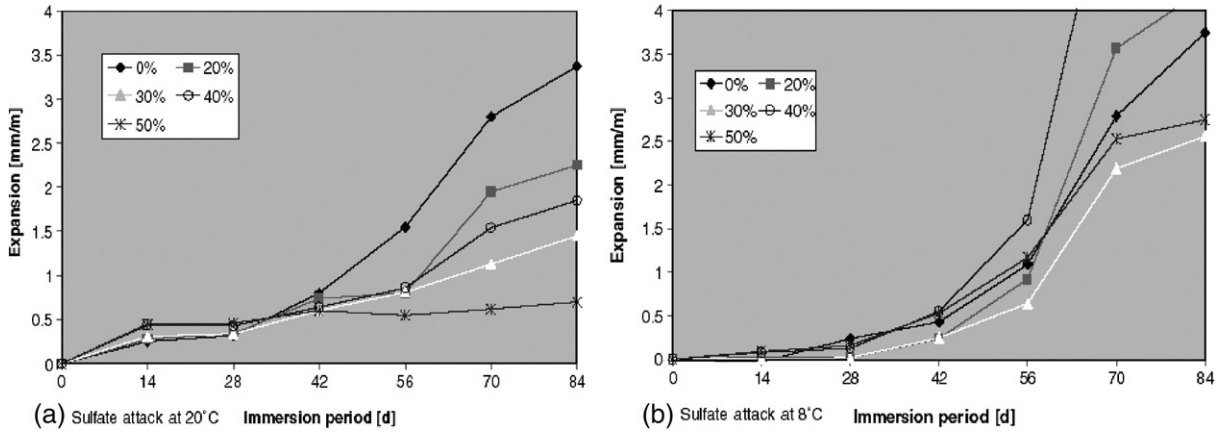

Fig. 15. Expansions of PLC mortar prisms containing fly ash after immersion in 4.4% sodium sulfate solution [123].

Table 3
Solubility constants of solid phases involved during sulfate ingress in hydrated cement systems [83]

Name	Chemical formula	Expression for equilibrium (K_{sp})	$-\log K_{sp}$
Ettringite	$3CaO{\cdot}Al_2O_3{\cdot}3CaSO_4{\cdot}32H_2^O$	$\{Ca^{2+}\}^6\{OH^-\}^4\{SO_4^{2}\}^3\{Al(OH)_4^-\}^2$	44.0
Monosulfate	$3CaO{\cdot}Al_2O_3{\cdot}CaSO_4{\cdot}12H_2O$	$\{Ca^{2+}\}^4\{OH^-\}^4\{SO_4^{2-}\}\{Al(OH)_4^-\}^2$	29.4
Gypsum	$CaSO_4{\cdot}2H_2O$	$\{Ca^{2+}\}\{SO_4^{2-}\}$	4.6

The ability of empirical and mechanistic models to predict the behavior of concrete structures under sulfate attack remains somewhat limited. Ionic transport modeling offer a more detailed description of the process through dissolution–precipitation reactions coupled to transport of ions in cementitious matrix [see Eq. (8))]. It is important to note that these models are inherently more complex than, for example, those used to describe chloride penetration. Sulfate, reacts more strongly with cement substances and models need therefore to include mineralogical transformations. The complexity of the problem is increased by the fact that concrete structures in contact with a sulfate-bearing solution can not only be subjected to sulfate attack but are also usually affected by decalcification. The chemical reactions occurring under sulfate attack can be summarized by the solubility constants of ettringite, monosulfate and gypsum given in Table 3 [83].

Simulations of the chemical degradation by sodium sulfate solutions were presented by Maltais et al. (Fig. 16b) [83]. As mentioned previously, the penetration of sulfate ions in cement-based materials can lead to the formation of a layer of gypsum at the vicinity of the exposed surface as shown in Fig. 16a. As can be seen in Fig. 16b, the multi-ionic model used by the authors could not only reproduce the sulfate distribution across the sample but was also capable to reliably predict the distribution of all other solid phases within the material. These results provide a good example of the potential of numerical modeling to investigate the behavior of cement-based materials exposed to chemically-aggressive environments.

7. Conclusions and perspectives

Since the last Congress, it has become more widely appreciated that (i) the real cost of concrete construction is partly dependant on service life and (ii) that the CO_2 emissions associated with cement production need to be reduced. While a wide range of responses to these challenges are being developed, performance lifetime is an important factor in offsetting the emissions associated with cement production and use and improving the competitiveness of concrete construction.

Of course not all structures need have long service lives but the tendency worldwide has been towards increased expectation of performances, subject to periodic inspection and maintenance.

However it is not easy to prove that a designated target service life can be achieved. We have historic examples of long-lived concrete but these may be of marginal relevance: many factors such as cement compositions, grain size distribution and mix design have changed. Yet, if concrete is to be regarded as an engineered material with controlled properties, it is essential to predict and assure its future performance. But this is easier said than done.

Performance has traditionally been measured empirically, by test protocols designed to simulate certain aggressive environments. An example is testing for sulfate resistance, where it has become standard to use aqueous sodium sulfate as the attacking agent. But empirical testing protocols suffer from a failure to analyze the physical and chemical basis of the test with sufficient rigor. Moreover the tests conditions are inflexible; results cannot be extrapolated or extended to conditions other than those imposed by specification with the result that, with few exceptions, empirical tests do not achieve a realistic predictive capability.

Many suggestions have been made for accelerated tests, for example, using ammonium salt solutions to accelerate leaching. But it is doubtful if results of these accelerated tests can be extrapolated, and the extrapolation justified, to the varied natural environments in which concretes undergo leaching.

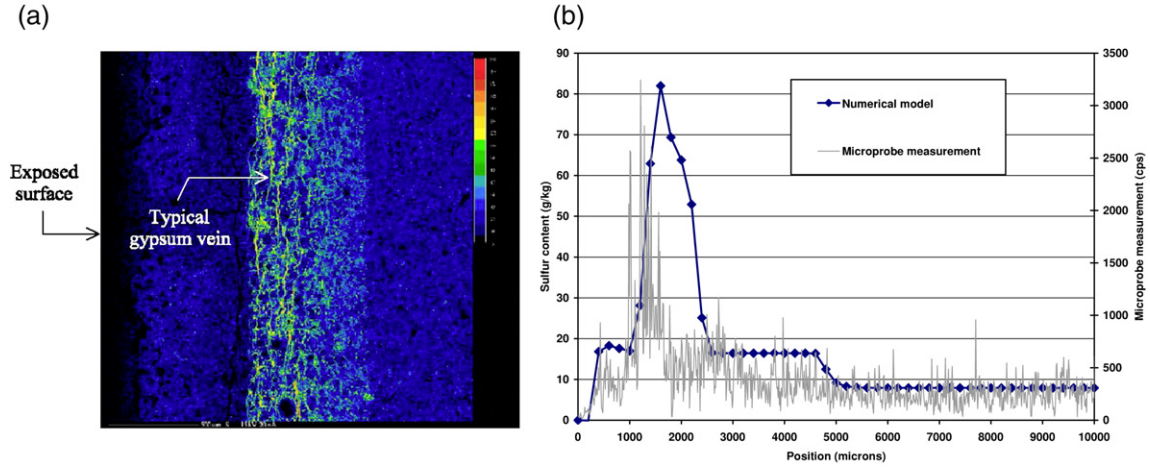

Fig. 16. Sulfur content mapping (a) and sulfur profiles (b) for 0.6 W/C ratio CSA Type 10 cement pastes exposed for 3 months to a 50 mmol/l Na_2SO_4 solution [83].

An alternative approach is to construct and apply models. We described these approaches. The models most attractive to engineers include dynamic features of cement performance; they allow for mass transport into and out of the solid matrix and calculate the resulting impacts. These models are based on physical chemistry which enforces a rigorous discipline on developers. Once developed, these models are inherently capable of great flexibility with regard to input parameters: time, temperature, cement composition, water composition, etc.

The state of development of modeling is described. Models contain essentially three aspects (i) a transport term, implying a kinetic description of the process or processes being modeled, (ii) a descriptive function, enabling the impact of, mass gains and losses to be expressed in terms of mineralogy, specific volume of solids, pH change, etc., and (iii) a mechanical property module, relating changes in engineering properties such as compressive strength, dimension, porosity, etc. to be calculated.

Progress towards modeling has been uneven, with some aspects being well developed but others lagging. Nevertheless the inherent ability of models, to embrace a wide range of user-designated compositions and temperatures, as well as the ability to compress the time factor suggests that, in the longer term, this approach will offer the greatest rewards. We therefore emphasise this approach believing that it offers the best way forward.

Modeling does not mean the end of experimental science; far from it. We highlight many areas where more data are needed. The best results are often achieved by combining targeted experiments with modeling. In this way, predictions can be tested to give user confidence and numerical values necessary to implement modelling can be obtained as needed.

Finally we note that an area requiring focussed and quantified development includes the integration of the traditional engineering property set with the body of knowledge concerning the chemical, mineralogical and microstructural properties of cement and concrete. Development of these links is becoming increasingly active.

We look forward to the transition of durability-related research from its present empirical state to a quantitative basis. We expect rapid progress to be reported at the next Congress. The payback will be to make cement and concrete a more environmentally friendly and sustainable class of materials and achieve more affordable construction, with concomitant social benefits.

Acknowledgements

The authors are grateful to Dr. Pierre Henocq for his invaluable contribution to the preparation of this paper. The authors would also like to acknowledge the financial support of the Canada Research Chair program and the Natural Sciences and Engineering Research Council of Canada.

References

[1] J.O'M. Bockris, A.K.N. Reddy, Modern Electrochemistry — An Introduction to an Interdisciplinary Area, Plenum Press, USA, 1970.
[2] F. Helfferich, Ion exchange, McGraw-Hill, USA, 1961.
[3] E. Samson, J. Marchand, Modeling the effect of temperature on ionic transport in cementitious materials, Cement and Concrete Research 37 (2007) 455–468.
[4] O. Sten-Knudsen, Biological Membranes — Theory of transport, potentials and electric impulses, Cambridge University Press, UK, 2002.
[5] J.F. Pankow, Aquatic Chemistry Concepts, Lewis Publishers, USA, 1994.
[6] A. Hidalgo, G. De Vera, M.A. Climent, C. Andrade, C. Alonso, Measurements of chloride activity coefficients in real Portland cement paste pore solutions, Journal of the American Ceramic Society 84 (2001) 3008–3012.
[7] E.J. Reardon, Problems and approaches to the prediction of the prediction of the chemical composition in cement/water systems, Waste Management 12 (1992) 221–239.
[8] E.J. Reardon, An ion interaction model for the determination of chemical equilibria in cement/water systems, Cement and Concrete Research 20 (1990) 175–192.
[9] E. Samson, G. Lemaire, J. Marchand, J.J. Beaudoin, Modeling chemical activity effects in strong ionic solutions, Computational Materials Science 15 (1999) 285–294.
[10] L.Y. Li, C.L. Page, Modelling of electrochemical chloride extraction from concrete: influence of ionic activity coefficients, Computational Materials Science 9 (1998) 303–308.
[11] J. Bear, Y. Bachmat, Introduction to Modeling of Transport Phenomena in Porous Media, Kluwer Academic Publishers, The Netherlands, 1991.
[12] M. Hassanizadeh, W.G. Gray, General conservation equations for multi-phase systems: 1. Averaging procedure, Advances in Water Resources 2 (1979) 131–144.
[13] E. Samson, J. Marchand, K.A. Snyder, J.J. Beaudoin, Modeling ion and fluid transport in unsaturated cement systems in isothermal conditions, Cement and Concrete Research 35 (2005) 141–153.
[14] B.F. Johannesson, A theoretical model describing diffusion of a mixture of different types of ions in pore solution of concrete coupled to moisture transport, Cement and Concrete Research 33 (2003) 481–488.
[15] K.T.B. MacQuarrie, K.U. Mayer, Reactive transport modeling in fractured rock: a state-of-the-science review, Earth-Science Reviews 72 (2005) 189–227.
[16] J. Simunek, D.L. Suarez, Two-dimensional transport model for variably saturated porous media with major ion chemistry, Water Resources Research 30 (1994) 1115–1133.
[17] S. Emmanuel, B. Berkowitz, Mixing-induced precipitation and porosity evolution in porous media, Advances in water resources 28 (2005) 337–344.
[18] J.M. Zalc, S.C. Reyes, E. Iglesia, The effects of diffusion mechanism and void structure on transport rates and tortuosity factors in complex porous structures, Chemical Engineering Science 59 (2004) 2947–2960.
[19] A. Saetta, R. Scotta, R. Vitaliani, Analysis of chloride diffusion into partially saturated concrete, ACI Materials Journal 90 (1993) 441–451.
[20] M.D.A. Thomas, Modeling chloride diffusion in concrete — effect of fly ash and slag, Cement and Concrete Research 29 (1999) 487–495.
[21] E. Samson, J. Marchand, Multiionic approaches to model chloride binding in cementitious materials, in: J. Marchand, et al., (Eds.), 2nd Int. Symp. On Advances in Concrete through Science and Engineering, RILEM Proceedings vol. 51, RILEM Publications, France, 2006.
[22] M. Mainguy, O. Coussy, V. Baroghel-Bouny, Role of air pressure in drying of weakly permeable materials, Journal of Engineering Mechanics 127 (2001) 582–592.
[23] A. Degiovanni, C. Moyne, Conductivité thermique de matériaux poreux humides: évaluation théorique et possibilité de mesure, International Journal of Heat and Mass Transfer 30 (1987) 2225–2245 (in French).
[24] J. Selih, A.C.M. Sousa, T.W. Bremner, Moisture transport in initially fully saturated concrete during drying, Transport in Porous Media 24 (1996) 81–106.
[25] S. Whitaker, Coupled transport in multiphase systems: a theory of drying, in: J.P. Hartnett, et al., (Eds.), Advances in Heat Transfer, 31, 1998, pp. 1–104.
[26] C. Hall, Barrier performance on concrete: a review of fluid transport theory, Materials and Structures 27 (1994) 291–306.
[27] Z.P. Bazant, L.J. Najjar, Drying of concrete as a nonlinear diffusion problem, Cement and Concrete Research 1 (1971) 461–473.

[28] Y. Xi, Z.P. Bazant, L. Molina, H.M. Jennings, Moisture diffusion in cementitious materials — Moisture capacity and diffusivity, Advanced Cement Based Materials 1 (1994) 258–266.
[29] O. Truc, J.P. Ollivier, L.O. Nilsson, Numerical simulation of multi-species diffusion, Materials and Structures 33 (2000) 566–573.
[30] M. Masi, D. Colella, G. Radaelli, L. Bertolini, Simulation of chloride penetration in cement-based materials, Cement and Concrete Research 27 (1997) 1591–1601.
[31] B.A. Schrefler, Multiphase flow in deforming porous material, International Journal for Numerical Methods in Engineering 60 (2004) 27–50.
[32] B. Martín-Pérez, S.J. Pantazopoulou, M.D.A. Thomas, Numerical solution of mass transport equations in concrete structures, Computers and Structures 79 (2001) 1251–1264.
[33] F. Barberon, V. Baroghel-Bouny, H. Zanni, B. Bresson, J.-B. d'Espinose de la Caillerie, L. Malosse, G. Zehong, Interactions between chloride and cement paste materials, Magnetic Resonance Imaging 23 (2005) 267–272.
[34] P.W. Brown, S. Badger, The distribution of bound sulfates and chlorides in concrete subjected to mixed NaCl, $MgSO_4$, Na_2SO_4 attack, Cement and Concrete Research 30 (2000) 1535–1542.
[35] P. Brown, J. Bothe, The system $CaO–Al_2O_3–CaCl_2–H_2O$ at 23±2 °C and the mechanisms of chloride binding in concrete, Cement and Concrete Research 34 (2004) 1549–1553.
[36] T.U. Mohammed, H. Hamada, T. Yamaji, Concrete after 30 years of exposure — Part I: mineralogy, microstructure and interfaces, ACI Materials Journal 101 (2004) 3–12.
[37] A.K. Suryavanshi, J.D. Scantlebury, S.B. Lyon, Mechanism of Friedel's salt formation in cement rich in tri-calcium aluminate, Cement and Concrete Research 26 (1996) 717–772.
[38] U.A. Birnin-Yauri, F.P. Glasser, Friedel's salt, $Ca_2Al(OH)_6(Cl,OH)·H_2O$: its solid solutions and their role in chloride binding, Cement and Concrete Research 28 (1998) 1713–1723.
[39] F.P. Glasser, A. Kindness, S.A. Stronach, Stability and solubility relationships in AFm phases Part I. Chloride, sulfate and hydroxide, Cement and Concrete Research 29 (1999) 861–866.
[40] A.K. Suryavanshi, J.D. Scantlebury, S.B. Lyon, The binding of chloride ions by sulphate resistant Portland cement, Cement and Concrete Research 25 (1995) 581–592.
[41] J. Csizmadia, G. Balázs, F.D. Tamás, Chloride ion binding capacity of aluminoferrites, Cement and Concrete Research 31 (2001) 577–588.
[42] T. Luping, L.O. Nilsson, Chloride binding capacity and binding isotherms of OPC pastes and mortars, Cement and Concrete Research 23 (1993) 247–253.
[43] J.J. Beaudoin, V.S. Ramachandran, R.F. Feldman, Interaction of chloride and C–S–H, Cement and Concrete Research 20 (1990) 833–875.
[44] P. Henocq, J. Marchand, E. Samson, J.A. Lavoie, Modeling of ionic interactions at the C–S–H surface — Application to CsCl and LiCl solutions in comparison with NaCl solutions, in: J. Marchand, et al., (Eds.), 2nd Int. Symp. On Advances in Concrete through Science and Engineering, RILEM Proceedings vol. 51, RILEM Publications, France, 2006.
[45] Y. Maltais, J. Marchand, P. Henocq, T. Zhang, J. Duchesne, Ionic interactions in cement-based materials: importance of physical and chemical interactions in presence of chloride or sulfate ions, in: J.P. Skalny (Ed.), Materials Science of Concrete VII, American Ceramic Society, USA, 2004.
[46] S.Y. Hong, F.P. Glasser, Alkali binding in cement pastes Part I. The C–S–H phase, Cement and Concrete Research 29 (1999) 1893–1903.
[47] M.R. Jones, D.E. Macphee, J.A. Chudek, G. Hunter, R. Lannegrand, R. Talero, S.N. Scrimgeour, 'Studies using 27Al MAS NMR of Afm and Aft phases and the Freidel's salt', Cement and Concrete Research 33 (2003) 177–182.
[48] S. Munshi, M. Boulfiza, Chlorides ingress and carbonation: effect on partitioning between free and bound chlorides, In Proceedings of the ConMAT Conference, in: N. Banthia et al. (Eds.), University of British Columbia, Vancouver, Canada, 2005.
[49] Y. Hosokawa, K. Yamada, B.F. Johannesson, L.O. Nilsson, Models for chloride ion bindings in hardened cement paste using thermodynamic equilibrium calculations, in: J. Marchand, et al., (Eds.), 2nd Int. Symp. On Advances in Concrete through Science and Engineering, RILEM Proceedings PRO, vol. 51, RILEM Publications, Quebec City, Canada, 2006.
[50] P. Ghods, M. Chini, R. Alizadeh, M. Hoseini, The effect of different exposure conditions on the chloride diffusion into concrete in the Persian Gulf region, in: N. Banthia, et al., (Eds.), Proceedings of the ConMAT Conference, 2005, University of British Columbia, Vancouver (Canada).
[51] R.E. West, W.G. Hime, Chloride profiles in salty concrete, Materials Performance 24 (1985) 29–36.
[52] L. Tang, L.O. Nilsson, Chloride binding capacity and binding isotherms of OPC pastes and mortars, Cement and Concrete Research 23 (1993) 247–253.
[53] E.J. Hansen, V.E. Saouma, Numerical simulation of reinforced concrete deterioration — part 1: chloride diffusion, ACI Materials Journal 96 (1999) 173–180.
[54] M. Nagesh, B. Bhattacharjee, Modeling of chloride diffusion in concrete and determination of diffusion coefficients, ACI Materials Journal 95 (1998) 113–120.
[55] S. Swaddiwudhipong, S.F. Wong, T.H. Wee, S.L. Lee, Chloride ingress in partially and fully saturated concrete structures, Concrete Science and Engineering 2 (2000) 17–31.
[56] B.B. Hope, A.K. Ip, D.G. Manning, Corrosion and electrical impedance in concrete, Cement and Concrete Research 15 (1985) 525–534.
[57] C. Alonso, C. Andrade, C. Castellote, P. Castro, Chloride threshold values to depassivate reinforcing bars embedded in a standardized OPC mortar, Cement and Concrete Research 30 (2000) 1047–1055.
[58] G.K. Glass, N.R. Buenfeld, Presentation of the chloride threshold level for corrosion of steel in concrete, Corrosion Science 39 (1997) 1001–1013.
[59] D.A. Hausmann, Steel corrosion in concrete — How does it occur, Materials Protection 6 (1967) 19–23.
[60] Federal Highway Administration (FHWA), Corrosion Evaluation of Epoxy-coated, Metallic-clad and Solid Metallic Reinforcing Bars in Concrete, Report No. FHWA RD 98 153 (1998).
[61] K. Tuutti, Corrosion of steel in concrete, Swedish Cement and Concrete Research Institute. Report Fo 4:82, CBI, Stockholm. Sweden, 1982.
[62] C. Dow, F.P. Glasser, Calcium carbonate efflorescence on Portland cement and building materials, Cement and Concrete Research 33 (2003) 147–154.
[63] L.N. Plummer, E. Busenberg, The solubilities of calcite, aragonite and vaterite in $CO_2–H_2O$ solutions between 0 and 90 °C, and an evaluation of the aqueous model for the system $CaCO_3–CO_2$, Geochimica et Cosmochimica Acta 46 (1982) 1011–1040.
[64] T. Xu, J.A. Apps, K. Pruess, Numerical simulation of CO_2 disposal by mineral trapping in deep aquifers, Applied Geochemistry 19 (2004) 917–936.
[65] P. Barret, D. Bertrandie, D. Beau, Calcium hydrocarboaluminate, carbonate alumina gel and hydrated aluminates solubility diagram calculated in equilibrium with CO_2g and with Na^+aq ions, Cement and Concrete Research 13 (1983) 789–800.
[66] V.G. Papadakis, C.G. Vayenas, M.N. Fardis, Fundamental modeling and experimental investigation of concrete carbonation, ACI Materials Journal 88 (1991) 363–373.
[67] A. Saetta, B.A. Schrefler, R. Vitaliani, The carbonation of concrete and the mechanism of moisture, heat and carbon dioxide flow through porous materials, Cement and Concrete Research 23 (1993) 761–772.
[68] D. Damidot, S. Stronach, A. Kindness, M. Atkins, F.P. Glasser, Thermodynamic investigation of the $CaO–Al_2O_3–CaCO_3–H_2O$ closed system at 25 °C and the influence of Na_2O, Cement and Concrete Research 24 (1994) 563–572.
[69] D. Damidot, F.P. Glasser, Thermodynamic investigation of the $CaO–Al_2O_3–CaSO_4–CaCO_3–H_2O$ closed system at 25 °C and the influence of Na2O, Advance in Cement Research 7 (1995) 129–134.
[70] F.P. Glasser, T. Matschei, Interactions between Portland cement and carbon dioxide, Proceedings of the ICCC Conference, 2007, Montreal, Canada.
[71] G. Cultrone, E. Sebastian, M.O. Huertas, Forced and natural carbonation of lime-based mortars with and without additives:

mineralogical and textural changes, Cement and Concrete Research 35 (2005) 2278–2289.
[72] C.A. Rigo da Silva, R.J.P. Reis, F.S. Lameiras, W.L. Vasconcelos, Carbonation-related microstructural changes in long-term durability concrete, Materials Research 5 (2002) 287–293.
[73] Y.F. Houst, F.H. Wittmann, Depth profiles of carbonates formed during natural carbonation, Cement and Concrete Research 32 (2002) 1923–1930.
[74] V. Baroghel-Bouny, T. Chaussadent, Transferts dans les bétons et durabilité des ouvrages, Bulletin du Laboratoire Ponts et Chaussées 248 (2004) 93–111 (in French).
[75] B. Bary, A. Sellier, Coupled moisture – carbon dioxide – calcium transfer model for carbonation of concrete, Cement and Concrete Research 34 (2004) 1859–1872.
[76] J.H. Cahyadi, T. Uomoto, Influence of environmental relative humidity on carbonation on concrete (mathematical modeling), in: S. Nagataki (Ed.), Durability of Building Materials and Components 6, 1993, pp. 1142–1151.
[77] A.V. Saetta, R.V. Vitaliani, Experimental investigation and numerical modeling of carbonation process in reinforced concrete structures Part I: theoretical formulation, Cement and Concrete Research 34 (2004) 571–579.
[78] H.W. Song, S.J. Kwon, K.J. Byun, C.K. Park, Predicting carbonation in early-aged cracked concrete, Cement and Concrete Research 36 (2006) 979–989.
[79] H.A.F. Dehwah, Effect of sulfate concentration and associated cation type on concrete deterioration and morphological changes in cement hydrates, Construction and Building Materials 21 (2007) 29–39.
[80] P. Faucon, P. Le Bescop, F. Adenot, P. Bonville, J.F. Jacquinot, P. Pineau, B. Felix, Leaching of cement: study of the surface layer, Cement and Concrete Research 26 (11) (1996) 1707–1715.
[81] K. Haga, S. Sutou, M. Hironaga, S. Tanaka, S. Nagasaki, Effects of porosity on leaching of Ca from hardened ordinary portland cement paste, Cement and Concrete Research 35 (2005) 1764–1775.
[82] M. Mainguy, C. Tognazzi, J.-M. Torrenti, F. Adenot, Modelling of leaching in pure cement paste and mortar, Cement and Concrete Research 30 (2000) 83–90.
[83] Y. Maltais, E. Samson, J. Marchand, Predicting the durability of Portland cement systems in aggressive environments — laboratory validation, Cement and Concrete Research 34 (2004) 1579–1589.
[84] A. Hidalgo, S. Petit, C. Domingo, C. Alonso, C. Andrade, Microstructural characterization of leaching effects in cement pastes due to neutralisation of their alkaline nature — Part I: Portland cement pastes, Cement and Concrete Research 37 (2007) 63–70.
[85] K. Yokozeki, K. Watanabe, N. Sakata, N. Otsuki, Modeling of leaching from cementitious materials used in underground environment, Applied Clay Science 26 (2004) 293–308.
[86] C. Carde, R. François, J.M. Torrenti, Leaching of both calcium hydroxide and C–S–H from cement paste: modeling the mechanical behavior, Cement and Concrete Research 26 (8) (1996) 1257–1268.
[87] C. Carde, R. François, Aging damage model of concrete behavior during the leaching process, Materials and Structures 30 (1997) 465–472.
[88] T. Matschei, B. Lothenbach, F.P. Glasser, The AFm phase in Portland cement, Cement and Concrete Research 37 (2007) 118–130.
[89] A. Bertron, J. Duchesne, G. Escadeillas, Accelerated tests of hardened cement pastes alteration by organic acids: analysis of the pH effect, Cement and Concrete Research 35 (2005) 155–166.
[90] H. Saito, A. Deguchi, Leaching tests on different mortars using accelerated electrochemical method, Cement and Concrete Research 30 (2000) 1815–1825.
[91] P. Faucon, F. Adenot, M. Jorda, R. Cabrillac, Behaviour of crystallised phases of Portland cement upon water attack, Materials and Structures 30 (1997) 480–485.
[92] P. Faucon, F. Adenot, J.F. Jacquinot, J.C. Petit, R. Cabrillac, M. Jorda, Long-term behaviour of cement pastes used for nuclear waste disposal: review of physico-chemical mechanisms of water degradation, Cement and Concrete Research 28 (6) (1998) 847–857.
[93] F. Adenot, M. Buil, Modelling of the corrosion of the cement paste by deionized water, Cement and Concrete Research 22 (1992) 489–496.
[94] U.R. Berner, Evolution of pore water chemistry during degradation of ceemnt in a radioactive waste repository environment, Waste Management 12 (1992) 201–219.
[95] M. Andac, F.P. Glasser, Long-term leaching mechanisms of portland cement-stabilized municipal solid waste fly ash in carbonated water, Cement and Concrete Research 29 (1999) 179–186.
[96] M. Moranville, S. Kamali, E. Guillon, Physicochemical equilibria of cement-based materials in aggressive environments — experiment and modeling, Cement and Concrete Research 34 (2004) 1569–1578.
[97] H.F.W. Taylor, Cement Chemistry, Thomas Telford, London, 1997.
[98] S. Catinaud, J.J. Beaudoin, J. Marchand, Influence of limestone addition on calcium leaching mechanisms in cement-based materials, Cement and Concrete Research 30 (2000) 961–1968.
[99] D. Kuhl, F. Bangert, G. Meschke, Coupled chemo-mechanical deterioration of cementitious materials. Part I: modeling, International Journal of Solids and Structures 41 (2004) 15–40.
[100] M. Daimon, S.A. Abo-El-Enein, G. Hosaka, S. Goto, R. Kondo, Pore structure of calcium silicate hydrate in hydrated tricalcium silicate, Journal of the American Ceramic Society 60 (3–4) (1977) 110–114.
[101] S. Rémond, D.P. Bentz, P. Pimienta, Effects of the incorporation of municipal solid waste incineration fly ash in cement pastes and mortars — II: modeling, Cement and Concrete Research 32 (2002) 565–576.
[102] J. Marchand, D. Bentz, E. Samson, Y. Maltais, Influence of calcium hydroxide dissolution on the transport properties of hydrated cement systems, in: J.P. Skalny, et al., (Eds.), Materials Science of Concrete — Special Volume: Calcium Hydroxide in Concrete, American Ceramic Society, USA, 2001, pp. 113–129.
[103] J. Skalny, J. Marchand, I. Odler, Sulfate Attack on Concrete, Spon Press, New-York, 2002.
[104] D. Planel, J. Sercombe, P. Le Bescop, F. Adenot, J.M. Torrenti, Long-term performance of cement paste during combined calcium leaching-sulfate attack: kinetics and size effect, Cement and Concrete Research 36 (2006) 137–143.
[105] D.D. Higgins, Increased sulfate resistance of ggbs concrete in the presence of carbonate, Cement & Concrete Composites 25 (2003) 913–919.
[106] N.N. Naik, A.C. Jupe, S.R. Stock, A.P. Wilkinson, P.L. Lee, K.E. Kurtis, Sulfate attack monitored by microCT and EDXRD: influence of cement type, water-to-cement ratio, and aggregate, Cement and Concrete Research 36 (2006) 144–159.
[107] B. Tian, M.D. Cohen, Does gypsum formation during sulfate attack on concrete lead to expansion? Cement and Concrete Research 30 (2000) 117–123.
[108] C. Ouyang, A. Nanni, W.F. Chang, Internal and external sources of sulfate ions in portland cement mortar: two types of chemical attack, Cement and Concrete Research 18 (1988) 699–709.
[109] S.T. Lee, H.Y. Moon, R.N. Swamy, Sulfate attack and role of silica fume in resisting strength loss, Cement & Concrete Composites 27 (2005) 65–76.
[110] T. Matschei, F.P. Glasser, The role of sodium sulfate in sulfate attack, Materials and Structures, in press.
[111] I. Odler, J. Colàn-Subauste, Investigations on cement expansion associated with ettringite formation, Cement and Concrete Research 29 (1999) 731–735.
[112] T. Bakharev, J.G. Sanjayan, Y.B. Cheng, Sulfate attack on alkali-activated slag concrete, Cement and Concrete Research 32 (2002) 211–216.
[113] N.M. Al-Akhras, Durability of metakaolin concrete to sulfate attack, Cement and Concrete Research 36 (2006) 1727–1734.
[114] J. Bensted, Thaumasite — bakground and nature in deterioration of cements, mortars and concretes, Cement & Concrete Composites 21 (1999) 117–121.
[115] T. Sibbick, D. Fenn, N. Crammond, The occurrence of thaumasite as a product of seawater attack, Cement & Concrete Composites 25 (2003) 1059–1066.
[116] S. Diamond, Thaumasite in Orange County, Southern California: an inquiry into the effect of low temperature, Cement & Concrete Composites 25 (2003) 1161–1164.

[117] M. Romer, L. Holzer, M. Pfiffner, Swiss tunnel structures: concrete damage by formation of thaumasite, Cement & Concrete Composites 25 (2003) 1111–1117.
[118] M. Collepardi, Thaumasite formation and deterioration in historic buildings, Cement & Concrete Composites 21 (1999) 147–154.
[119] G. Collet, N.J. Crammond, R.N. Swamy, J.H. Sharp, The role of carbon dioxide in the formation of thaumasite, Cement and Concrete Research 34 (2004) 1599–1612.
[120] M. Santhanam, M.D. Cohen, J. Olek, Sulfate attack research, Cement and Concrete Research 31 (2001) 845–851.
[121] J. Aguilera, S. Martinez-Ramirez, I. Pajarez-Colomo, M.T. Blanco-Varela, Formation of thaumasite in carbonated mortars, Cement & Concrete Composites 25 (2003) 991–996.
[122] P. Nobst, J. Stark, Investigations on the influence of cement type on thaumasite formation, Cement & Concrete Composites 25 (2003) 899–906.
[123] D.M. Mulenga, J. Stark, P. Nobst, Thaumasite formation in concrete and mortars containing fly ash, Cement & Concrete Composites 24 (2003) 907–912.
[124] S. Tsivilis, G. Kakali, A. Skaropoulou, J.H. Sharp, R.N. Swamy, Use of mineral admixtures to prevent thaumasite formation in limestone cement mortar, Cement & Concrete Composite 25 (2003) 969–976.
[125] F. Bellmann, B. Möser, J. Stark, Influence of sulfate solution concentration on the formation of gypsum in sulfate resistance test specimen, Cement and Concrete Research 36 (2006) 358–363.
[126] J. Hill, E.A. Byars, J.H. Sharp, C.J. Lynsdale, J.C. Cripps, Q. Zhou, An experimental study of combined acid and sulfate attack of concrete, Cement & Concrete Composites 25 (2003) 997–1003.
[127] Q. Zhou, J. Hill, E.A. Byars, J.C. Cripps, C.J. Lynsdale, J.H. Sharp, The role of pH in thaumasite sulfate attack, Cement and Concrete Research 36 (2006) 160–170.
[128] P. Brown, R.D. Hooton, Ettringite and thaumasite formation in laboratory concretes prepared using sulfate-resisting cements, Cement & Concrete Composite 24 (2002) 361–370.
[129] D.W. Hobbs, M.G. Taylor, Nature of the Thaumasite sulafte attack mechanism in field concrete, Cement and Concrete Research 30 (2000) 529–533.
[130] D.W. Hobbs, Thaumasite sulfate attack in field and laboratory concretes: implications for specifications, Cement & Concrete Composites 25 (2003) 1195–1202.
[131] N. Loudon, A review of the experience of thaumasite sulfate attack by the UK Highways Agency, Cement & Concrete Composites 25 (2003) 1051–1058.
[132] D.E. Macphee, S.J. Barnett, Solution properties of solids in the ettringite–thaumasite solid solution series, Cement and Concrete Research 34 (2004) 1591–1598.
[133] I. Juel, D. Herfort, R. Gollop, J. Konnerup-Madsen, H.J. Jakobsen, J. Skibsted, A thermodynamic model for predicting the stability of thaumasite, Cement & Concrete Composites 25 (2003) 867–872.
[134] K.E. Kurtis, P.J.M. Monteiro, S. Madanat, Empirical models to predict concrete expansion caused by sulfate attack, ACI Materials Journal V97 (March–April 2000) 156–161 Errata published November–December 2000, V97 713.
[135] J. Marchand, E. Samson, Y. Maltais, J.J. Beaudoin, Theoretical analysis of the effect of weak sodium sulfate solutions on the durability of concrete, Cement & Concrete Composites 24 (2002) 317–329.
[136] T. Ishida, K. Kawai, R. Sato, Experimental study on decomposition processes of Friedel's salt due to carbonation, in: K. Kovler (Ed.), Proc. Int. RILEM-JCI Seminar on Concrete Durability (ConcreteLife'06), 2006, pp. 51–58, Ein-Bokek (Israel).
[137] I. Pajares, S. Martinez-Ramirez, M.T. Blanco-Varela, Evolution of ettringite in presence of carbonate, and silicate ions, Cement & Concrete Composites 25 (2003) 861–865.
[138] D. Heinz, L. Urbonas, About thaumasite formation in Portland – limestone cement pastes and mortars – effect of heat treatment at 95 °C and storage at 5 °C, Cement & Concrete Composites 25 (2003) 961–967.